NASA / TM-2000-210540

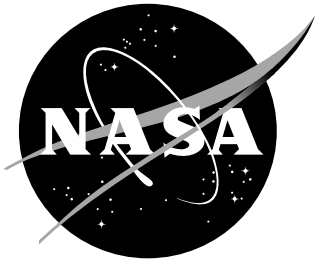

Microstructural and Mechanical Property Characterization of Shear Formed Aerospace Aluminum Alloys

Lillianne P. Troeger, Marcia S. Domack, and John A. Wagner
Langley Research Center, Hampton, Virginia

October 2000

The NASA STI Program Office ... in Profile

Since its founding, NASA has been dedicated to the advancement of aeronautics and space science. The NASA Scientific and Technical Information (STI) Program Office plays a key part in helping NASA maintain this important role.

The NASA STI Program Office is operated by Langley Research Center, the lead center for NASA's scientific and technical information. The NASA STI Program Office provides access to the NASA STI Database, the largest collection of aeronautical and space science STI in the world. The Program Office is also NASA's institutional mechanism for disseminating the results of its research and development activities. These results are published by NASA in the NASA STI Report Series, which includes the following report types:

- TECHNICAL PUBLICATION. Reports of completed research or a major significant phase of research that present the results of NASA programs and include extensive data or theoretical analysis. Includes compilations of significant scientific and technical data and information deemed to be of continuing reference value. NASA counterpart of peer-reviewed formal professional papers, but having less stringent limitations on manuscript length and extent of graphic presentations.

- TECHNICAL MEMORANDUM. Scientific and technical findings that are preliminary or of specialized interest, e.g., quick release reports, working papers, and bibliographies that contain minimal annotation. Does not contain extensive analysis.

- CONTRACTOR REPORT. Scientific and technical findings by NASA-sponsored contractors and grantees.

- CONFERENCE PUBLICATION. Collected papers from scientific and technical conferences, symposia, seminars, or other meetings sponsored or co-sponsored by NASA.

- SPECIAL PUBLICATION. Scientific, technical, or historical information from NASA programs, projects, and missions, often concerned with subjects having substantial public interest.

- TECHNICAL TRANSLATION. English-language translations of foreign scientific and technical material pertinent to NASA's mission.

Specialized services that complement the STI Program Office's diverse offerings include creating custom thesauri, building customized databases, organizing and publishing research results ... even providing videos.

For more information about the NASA STI Program Office, see the following:

- Access the NASA STI Program Home Page at ***http://www.sti.nasa.gov***

- E-mail your question via the Internet to help@sti.nasa.gov

- Fax your question to the NASA STI Help Desk at (301) 621-0134

- Phone the NASA STI Help Desk at (301) 621-0390

- Write to:
  NASA STI Help Desk
  NASA Center for AeroSpace Information
  7121 Standard Drive
  Hanover, MD 21076-1320

NASA / TM-2000-210540

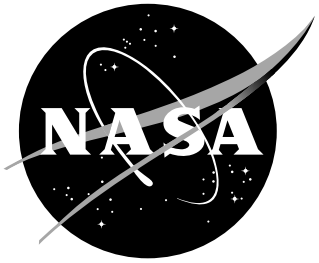

Microstructural and Mechanical Property Characterization of Shear Formed Aerospace Aluminum Alloys

Lillianne P. Troeger, Marcia S. Domack, and John A. Wagner
Langley Research Center, Hampton, Virginia

National Aeronautics and
Space Administration

Langley Research Center
Hampton, Virginia 23681-2199

October 2000

Available from:

NASA Center for AeroSpace Information (CASI)
7121 Standard Drive
Hanover, MD 21076-1320
(301) 621-0390

National Technical Information Service (NTIS)
5285 Port Royal Road
Springfield, VA 22161-2171
(703) 605-6000

Table of Contents

List of Tables

List of Figures

Abstract

Advanced manufacturing processes such as near-net-shape forming can reduce production costs and increase the reliability of launch vehicle and airframe structural components through the reduction of material scrap and part count and the minimization of joints. The current research is an investigation of the processing-microstructure-property relationships for shear formed cylinders of the Al-Cu-Li-Mg-Ag alloy 2195 for space applications and the Al-Cu-Mg-Ag alloy C415 for airframe applications. Cylinders which had undergone various amounts of shear-forming strain were studied to correlate the grain structure, texture, and mechanical properties developed during and after shear forming.

1. Introduction

Near-net-shape manufacturing technologies represent attractive alternatives to traditional machining methods for airframe and space structures [1]. The advantages of near-net-shape manufacturing include a reduction in material scrap (i.e., machining chips) and the elimination of thick-plate microstructures which can result in improved mechanical properties. Shear forming (also referred to as roll forming, flow turning, flow forming, or power spinning) is a near-net-shape manufacturing technique originally developed for steel in which seamless cylindrical structures are produced by reducing the wall thickness and extending the length of ring-shaped preforms, while holding the nominal diameter constant [2]. Diagrams of the two types of shear forming used in the current study, herein referred to as the counter-roller method and the mandrel method, are shown in Figure 1 [3]. In counter-roller shear forming, an opposing pair of rollers deforms the material on both the inner and outer surfaces. In mandrel shear forming, one roller deforms the outer surface while the inner surface is supported by a mandrel.

Potential aerospace applications for shear formed aluminum cylinders include launch vehicle cryotanks and airframe fuselage structures. Although shear forming is now commonly applied to alloys of steel, titanium, and nickel, the technology for shear forming aluminum alloys has only recently been developed. NASA Langley Research Center (LaRC) has been working closely with Ladish Co., Inc. of Cudahy, Wisconsin over the past several years to produce and characterize shear formed aluminum alloy cylinders for aerospace applications. This paper describes the application of shear forming to two aluminum alloys, one for space applications (alloy 2195) and the other for airframe applications (alloy C415). The mechanical properties of shear formed 2195 are compared with plate properties from the Space Shuttle Super Lightweight Tank (SLWT) program [4,5]. Shear formed C415 mechanical properties are compared with C415 sheet properties.

2. Materials and Cylinder Manufacture

2.1. 2195 Shear Formed Cylinders

Table 1 shows the shear formed cylinder and SLWT 2195 compositions, along with the registered 2195 composition range. It can be seen from Table 1 that the 2195 composition used in the shear forming investigation is slightly different from the 2195 SLWT plate composition. This is in part due to the fact that the ingot of 2195 used for the shear forming study was produced prior to the selection of the 2195 composition for the SLWT program. However, both 2195 compositions fall within the allowable composition range [6].

Table 1. 2195 Alloy Compositions. (Weight %)

2195 Product Form	Cu	Li	Mg	Ag	Zr	Al
Shear Formed Cylinder	3.90	1.00	0.34	0.30	0.14	Bal.
SLWT Plate [4]	4.00	1.00	0.40	0.40	0.12	Bal.
2195 Composition Range [6]	3.70-4.30	0.80-1.20	0.25-0.80	0.25-0.60	0.08-0.16	Bal.

The SLWT is integrally machined from 2195 thick plate. During this process, 80-90% of the material is lost as machining chips. Al-Li alloys such as 2195 are more expensive than conventional aluminum alloys. A near-net-shape manufacturing process would utilize the material more efficiently than the current integral machining approach since scrap would be minimized.

To produce a 2195 cylinder, an ingot of 2195 was converted to a billet from which a cylinder was back extruded and ring rolled to produce a hollow, cylindrical preform with a diameter of 168 inches (14 feet). The preform was progressively shear formed into a single cylinder with a stepped thickness profile of 0.375 inches, 0.25 inches, and 0.15 inches (the cylinder wall thickness after one, two, or three shear-forming passes, respectively). The cylinder was then parted into three segments which are hereafter referred to as cylinders D, A, and C, respectively. A summary of the cylinder thicknesses and shear-forming strains is presented in Table 2. The shear-forming strain is based upon the thinning of the cylinder wall and is calculated in a manner similar to that for strain in superplastically formed cone specimens [7-9]. The true strain for each shear-formed cylinder is then given by:

$$\varepsilon=\ln(t_0/t_f)$$

where t_0 and t_f are the initial and final wall thicknesses, respectively. After shear forming, the cylinders were solution heat treated by Ladish Co., Inc. and shipped to LaRC, where they were stored for several months at room temperature prior to thermomechanical processing and analysis. The as-received condition for the 2195 cylinders is thus the T4 temper, defined as solution heat treatment followed by cold work and natural aging [10].

Table 2. Summary of Alloy 2195 Cylinder Thicknesses and Shear-Forming Strains.

Total True Shear-Forming Strain $\varepsilon=\ln(t_0/t_f)$	Initial Thickness t_0 (in.)	Final Thickness t_f (in.)	Cylinder
0.69	0.75	0.38	D
1.10	0.38	0.25	A
1.61	0.25	0.15	C

2.2. C415 Shear Formed Cylinders

The shear formed cylinders of alloy C415 were manufactured using the mandrel method starting with a 100-pound ingot. The composition of the alloy is shown in Table 3 [11]. The shear formed cylinders were produced from one back-extruded cylinder that was sectioned to yield six cylindrical preforms. The preforms were then machined on the inner surface to fit the mandrel. Note that the C415 cylinders were not ring rolled prior to being shear formed, in contrast to the 2195 cylinders described

previously. The preforms were shear formed independently to wall thicknesses ranging from 0.25 inches (cylinder 1) to 0.07 inches (cylinder 6), all with inner diameters of approximately 10.5 inches.

Table 4 summarizes cylinder the thicknesses and true shear-forming strains. The cylinders are listed in order of increasing applied strain. The shear-forming strains shown in Table 4 were calculated from the initial (0.5 inches) and final cylinder thicknesses only, since the intermediate cylinder thicknesses were not assessed during processing. Cylinder 2 failed during its first shear-forming pass. Table 5 shows the approximate processing schedule as indicated by the roll gap settings d_0, d_1, etc., for the multi-pass shear forming of the C415 preforms.

Table 3. C415 Alloy Composition.

Cu	Mg	Ag	Zr	Mn	Fe	Si	Al
5.00	0.80	0.50	0.13	0.60	0.06	0.04	Bal.

Table 4. Summary of Alloy C415 Cylinder Thicknesses and Shear-Forming Strains.

(t_0=0.5 inches)

Total True Shear Forming Strain $\varepsilon=\ln(t_0/t_f)$	Wall Thickness, t_f (inches)	Cylinder
0.71	0.24	1
0.71	0.24	5
-	-	2
1.37	0.13	4
1.66	0.10	3
1.88	0.08	6

Table 5. Approximate Shear Forming Schedule for Alloy C415 Preforms, Based on Roll Gap Settings.

Cylinder	d_0 (in.) (Preforms)	d_1 (in.)	d_2 (in.)	d_3 (in.)	d_4 (in.)
1	0.50	0.38	0.25	-	-
5	0.50	0.38	0.25	-	-
2	0.50	-	-	-	-
4	0.50	0.30	0.10	-	-
3	0.50	0.35	0.20	0.10	-
6	0.50	0.38	0.24	0.12	0.07

The C415 shear formed cylinders were delivered to LaRC in the T3 temper, which consisted of solution heat treatment (50 minutes at 970 °F), water quench, and 3% stretch by Ladish. The stretch was accomplished through repetitive cold expansion of the cylinder diameter using a four-segment stretcher tool applied to the inner surface as shown in Figure 2. The tool was applied, released, rotated slightly, and reapplied to accomplish the required amount of stretch while maintaining a quasi-circular cross-section. After receipt by LaRC, the cylinders were stored at room temperature for approximately one year before further processing and testing were initiated.

3. Experimental Procedures

3.1. Thermomechanical Processing

3.1.1. 2195 Shear formed cylinders. The 2195 cylinders were sectioned into rectangular blanks which were approximately 3 inches wide (along the circumferential direction), spanning the entire axial length of each cylinder segment (~4-7 inches). To achieve a T8 temper, the blanks were solutionized for 30 minutes at 950°F, water quenched, axially stretched 3%, and aged for 36 hours at 290°F [12]. The samples were stored at -13°F between processing steps to prevent natural aging, which was shown by the authors to occur rapidly after solution heat treatment as indicated by hardness measurements. (The Rockwell B hardness increased from approximately 20 after solution heat treatment and water quenching to over 50 after 5 hours of natural aging for all three cylinder segments.)

3.1.2. C415 shear formed cylinders. Due to the curvature of the 10.5-inch-diameter C415 cylinders, flattening was required to facilitate thermomechanical processing and the machining of mechanical test specimens. Segments of the C415 cylinders were flattened using a 120 kip press and/or a rolling mill, with the rolling direction parallel to the circumferential direction of the cylinder. Due to the residual stresses in the T3 cylinders, it was not possible to completely flatten the material, though useful specimens were still obtained in most cases.

Since the solution heat treated and stretched C415 cylinders had been stored at room temperature for approximately one year, achievement of typical T8 mechanical properties by direct aging was uncertain. To investigate the effect of the extended room-temperature storage of the cylinders on subsequent mechanical properties, two procedures were applied to the shear formed cylinders after flattening. These were based on the standard T8 temper developed for C415 sheet products, which includes solutionizing, stretching, and aging for 24 hours at 325°F [13]. The first procedure involved aging the T3 cylinders for 24 hours at 325°F to produce a “direct-aged” T8 temper (representing the insertion of a more than year-long natural aging interval into the standard T8 treatment). The second procedure involved re-solutionizing, stretching ~3% circumferentially, and aging for 24 hours at 325°F (i.e., per the standard T8 treatment for sheet products) to produce a “reprocessed" T8 temper.

3.2. Optical Metallography

Metallographic sections were prepared by standard polishing techniques, followed by anodizing in Barker’s Reagent for 10-15 seconds using 15 volts DC. The samples were then viewed with cross-polarized light and photographed. The coordinate system adopted for reporting microstructural and mechanical property data for the cylinders is shown in Figure 3.

3.2.1. 2195 shear formed cylinders. The microstructure of cylinders D, A, and C in the T4 condition was examined on three orthogonal planes, referenced to the axial (A), radial (R) and circumferential (C) axes (the AR, RC, and AC planes), at depths of t/8, t/2, and 7t/8 below the outer cylinder surface as shown in Figure 2. In addition, cross-sectional AR planes were examined through the entire thickness from the outer surface to the inner surfaces of each cylinder. Full-thickness AR sections were also examined following solution heat treatment and T8 tempering.

3.2.2. C415 shear formed cylinders. In order to keep the size of the test matrix for the metallographic and texture studies manageable, only cylinders 1 and 6 were studied in detail since they bracketed the extreme values of shear-forming strain. In order to determine the uniformity of the microstructure after stretching, metallographic sections were taken from two locations relative to the marks left by the stretching tool during the final iteration of the stretching procedure. As shown in Figure

2, a location directly beneath one stretcher mark was denoted 0°, while that roughly halfway between two stretcher marks was denoted 45°. The three mutually orthogonal planes were examined at depths of t/8, t/2, and 7t/8 below the outer surface of the cylinder, as were full-thickness views of the AR planes. For cylinders 3 and 4, which represented intermediate shear-forming strain levels, only full-thickness views of the AR planes were examined.

3.3. Texture Analysis

Data was collected using an automated x-ray goniometer, and Orientation Distribution Function (ODF) plots were generated from pole figures using Philips PC-Texture software. An initial investigation designated the circumferential direction as the reference axis for the texture analysis. (The "rolling direction" is normally chosen as the reference axis for rolled products such as plate and sheet. In shear forming, the rolling direction is parallel to the circumferential axis.) However, the texture results using this orientation did not correlate with traditional texture features for FCC materials [14]. When the *axial* direction was chosen as the reference axis instead, identifiable texture trends were observed. Therefore, this orientation was adopted for all texture specimens.

3.3.1. 2195 shear formed cylinders. Texture samples were ground to a 600-grit finish and etched for 15 seconds in a NaOH solution (30 grams of NaOH in 270 milliliters of distilled water) at 150°F and desmutted in nitric acid. Data was obtained from AC planes of cylinders D, A, and C in the T4 condition at depths of t/8, t/2, and 7t/8 below the outer surface. The cylinders were re-evaluated after solution heat treatment at t/2 only. After processing to the T8 temper, data was obtained only for cylinder C at all three depths.

3.3.2. C415 shear formed cylinders. The texture of the C415 cylinders was evaluated in the T3 condition before and after flattening to determine whether the flattening procedures significantly altered the texture. Samples from cylinders 1 and 6 were prepared by grinding to a 600-grit finish, etching in Keller's etch, and desmutting in nitric acid. Data was obtained from the AC planes of cylinders 1 and 6, each at the 0° and 45° positions and at depths of t/8, t/2, and 7t/8. After flattening, the texture of cylinders 1 and 6 was re-evaluated for all three depths at the 0° location.

3.4. Mechanical Property Testing

Tensile properties were evaluated for both the 2195 and C415 shear formed cylinders, while fracture toughness was evaluated only for the C415 cylinders. Due to the small size of the tensile blanks, non-standard, subsize tensile specimens were machined after processing the blanks to the T8 temper. The tensile specimens had a gage length of 0.75 inches and were oriented parallel to either the axial or the circumferential direction of the cylinders.

Room-temperature tensile tests were conducted using a servohydraulic test machine in accordance with ASTM Standard E8 [15]. The crosshead displacement rate was 0.01 inches per minute and was increased to 0.05 inches per minute after 2% strain. Strain was measured using two back-to-back extensometers and fiducial mark analysis. The extensometers had 0.3-inch gage lengths and were mounted on the sides of the specimens; they were calibrated for 15% extension (0.045 inches displacement) at full scale. Fiducial marks were applied to the specimens, spaced 0.5 inches apart. The distance between the marks was measured after fracture by reassembling the specimens. Elongation determined using fiducial marks was calculated for selected specimens so as to preserve the maximum number of fracture surfaces for future analysis. Back-to-back strain gages were also applied to selected specimens for validation of the elastic portion of the extensometer data. The elastic modulus determined from the extensometers and strain gages agreed within 2%, so use of the strain gages was discontinued for the remaining tests.

3.4.1. 2195 shear formed cylinders. The tensile specimens from cylinders D, A, and C were 0.1 inches thick and machined from the midthickness of the T8 blanks. Two axial and two circumferential specimens were tested from each cylinder. In addition to the back-to-back extensometers, back-to-back strain gages were applied to the axial specimens. The elastic modulus was computed from the stress-strain data over the approximate range of 0.1% and 0.3% nominal strain.

Due to problems with the extensometers on the circumferential specimens, valid modulus and yield strength data were obtained for only one of the circumferential specimens per cylinder. All other reported data is averaged over duplicate specimens.

The 2195 tensile specimens often fractured outside the extensometer gage length; therefore, ductility based on the extensometer data is not presented. However, elongations determined using the fiducial marks from one specimen per condition are included.

3.4.2. C415 shear formed cylinders. Since the C415-T3 cylinders could not be completely flattened, the subsequent T8 blanks exhibited residual waviness. This fact combined with the desire to sample as much of the through-thickness microstructure as possible led to different approaches for the selection of specimen thicknesses for cylinders 1 and 6.

Blanks from cylinder 1 were sufficiently flat and thick enough to allow the removal of approximately 0.02 inches from each side of the blank, resulting in 0.2-inch-thick test specimens with parallel faces. However, the waviness of the blanks from cylinder 6 coupled with its non-uniform microstructure made it necessary to machine full-thickness specimens from it. Machining the blanks to produce samples with parallel faces would not necessarily have represented the true microstructure since it varied markedly through the thickness for that cylinder.

Axial and circumferential tensile specimens were machined from cylinders 1 and 6 after direct-aging or reprocessing to the T8 temper. Triplicate tensile specimens were tested for each condition and orientation. In addition to the back-to-back extensometers, back-to-back strain gages were applied to two axial and two circumferential specimens from direct-aged cylinder 1, and to two axial specimens from reprocessed cylinder 6 for validation of the elastic portion of the extensometer data, as described previously.

The fracture toughness of cylinder 1 was evaluated in both the direct-aged and reprocessed conditions using compact tension (CT) specimens, oriented such that the specimen was loaded in the axial direction with crack propagation in the circumferential direction (AC orientation). The CT specimens were 2.0 inches wide and 0.20 inches thick after machining to produce parallel specimen surfaces. (It was not possible to obtain CT specimens from cylinder 6 due to the residual waviness of the blanks.) Fracture toughness was determined by the J-integral method in accordance with ASTM E1152-87 with physical crack length determined by the potential drop method [16]. The resulting J-R curves were converted to K-R curves using the relation:

$$K_I = [(J \times E)/(1-\upsilon^2)]^{1/2}$$

where J is the J-integral value, E is Young's Modulus, and υ is Poisson's ratio [17]. Initiation toughness was estimated from J_{Ic} in accordance with E813-89 for each condition [18]. K_{JIc} values were then calculated from J_{Ic}. Crack growth resistance was defined in this study as the K value at 0.15 inches of physical crack extension, $K_{0.15}$.

4. Results and Discussion

4.1. 2195 Shear Formed Cylinders

Macroscopic examination revealed surface cracks through the oxide layer on the inner surfaces of the 2195 cylinder segments. The cracks were aligned with the circumferential direction and were

probably the result of inadequate lubrication during the shear forming process. They were easily ground out and did not affect metallographic or texture results.

4.1.1. Microstructure. Examination of anodized samples of the 2195-T4 material indicated a partially recrystallized grain structure. Grains without substructure were interpreted as recrystallized grains. For cylinder D, which experienced the least amount of shear-forming strain, the grain structure was generally homogeneous through the thickness of the material. Elongated grains, with and without substructure, were interspersed with larger, less elongated, recrystallized grains, as seen in the midthickness triplanar view shown in Figure 4. Deformation bands were visible for cylinders D and A, as exemplified by those on the AC plane of cylinder D shown in Figure 4. In Figure 5, rows of grains oriented nearly 45° to the circumferential direction were observed near the outer surface of the cylinder. Numerous large, recrystallized grains on the AC plane are also elongated approximately 45° to the circumferential direction. These effects may have resulted from the mutually perpendicular deformation axes inherent to shear forming (axial extrusion superimposed upon circumferential rolling).

The grain structure of cylinders A and C was less homogeneous through the thickness than that of cylinder D. As shown in Figure 6, this inhomogeneity was most pronounced for cylinder C, which had experienced the greatest amount of shear-forming strain. While recrystallized areas were visible throughout the material, the outer surface region contained a smaller fraction of recrystallized grains; the inner region appeared to be more recrystallized with fine, equiaxed grains. The grain size tended to become more refined toward the inner surface regions. Large recrystallized grains were visible throughout the thickness.

The observation that the inner regions of the cylinders tended to show more recrystallization than the outer regions at larger shear-forming strains suggests that the deformation was concentrated at the inner portion of the cylinders during shear forming. This would increase the driving force for recrystallization in that area during subsequent solution heat treatment, resulting in a higher degree of recrystallization for the inner region of the cylinder (and thus a refined microstructure) relative to the outer region. After the material was resolutionized, stretched, and aged to the T8 temper, the grain structure remained largely unchanged.

4.1.2. Texture. The reader is referred to [14] and [19-20] for general discussions of texture and ODF's. There were four objectives for the texture analysis. The first was to investigate the texture in general, and to determine whether it was uniform through the thickness of the material. The second was to determine whether the texture characteristics were symmetrical about the midplane. The third was to determine the effect of increasing shear-forming strain on the texture and its intensity. The fourth was to determine whether the texture could be correlated with the mechanical property data.

The shear forming process involves a mixture of circumferential rolling and axial (longitudinal) extrusion. Consequently, it was difficult to define the principal deformation direction for the texture analysis. After some initial tests, it was concluded that meaningful data could only be obtained if the *axial* direction was defined as the principal deformation axis. By choosing the axial direction as the reference axis, rolling- and extrusion-type texture fibers and components could be identified in the ODF plots. The fact that FCC deformation texture features appeared for data referenced to the axial direction, but not for the circumferential direction, indicated that the dominant material deformation axis was parallel to the axial direction for the shear-forming process, even though the effective rolling direction was parallel to the circumferential direction. Additional analyses showed that there was no appreciable change in the texture after processing the T4 cylinders to the T8 temper. Therefore, texture data is only presented for the T4 material.

Texture data can be described in terms of texture fibers or specific texture components. The former proved to be the most useful in describing the overall texture characteristics for the shear formed cylinders. For relatively high levels of shear-forming strain (ε=1.6), the nature of the texture is best described as a deformation fiber texture which varied in orientation and intensity.

The orientation of the fiber varied through the thickness and was not symmetrical about the midplane. For high levels of shear-forming strain (cylinder C, ε=1.61), Figure 7 shows that near the outer surface (t/8) the texture most closely resembled a rolling-type fiber, similar to a β or {hkl}<112> fiber (originating at the Bs component). Near the inner surface (the 7t/8 location, shown in Figure 8), the fiber was closer to a cross-rolled orientation with {hkl}<322> (originating at the X-R component). At the midplane (Figure 9), the fiber had an orientation intermediate between the cross-rolled and extruded orientations (Ex_1), the latter having {hkl}<111>. The fiber was never centered on the extrusion fiber location. It can be seen that the deformation fiber is not well defined for low levels of shear forming strain (ε=0.69, Figure 10) but is strongly defined for higher levels (ε=1.61, Figure 8a). The overall texture intensity tended to be highest at the 7t/8 location regardless of level of shear forming strain.

Previous work suggests that yield strength is the only mechanical property which can be correlated with texture [21]. For the 2195 shear formed cylinders, the midthickness axial (longitudinal) yield strength was greater than the circumferential (transverse) yield strength, similar to 2195 rolled products and thick section extrusions [22]. (The yield strengths are shown in Table 6 and will be discussed in the next section.) The axial/circumferential yield strength differential increased with overall texture intensity, i.e., the yield strength anisotropy increased with shear-forming strain.

4.1.3. Tensile properties. A summary of the tensile behavior of the 2195-T8 shear formed cylinders is shown in Table 6. Results are presented for each cylinder in both the axial (A) and circumferential (C) orientations.

Table 6. Tensile Properties for 2195-T8 Shear Formed Cylinders.

Cylinder	ε	Orientation	E (Msi)	YS (ksi)	UTS (ksi)	% Elongation (Fiducial Marks)
D	0.69	A	10.7	56.6	72.3	24.6
		C	10.8	51.7	68.6	27.3
A	1.10	A	10.9	70.7	79.4	18.9
		C	10.8	60.9	69.6	24.4
C	1.61	A	11.0	71.8	79.9	18.8
		C	10.8	61.5	73.2	22.7

The elastic modulus remained essentially constant regardless of orientation or level of shear-forming strain, averaging 10.8 Msi. The effect of shear-forming strain on the yield and ultimate tensile strengths (YS and UTS, respectively) for the 2195-T8 cylinders is shown in Figure 11 for both the axial and circumferential orientations. Typical strength properties for 2195-T8 plate (SLWT composition) are shown for comparison [5]. Both the axial and circumferential yield and tensile strengths increased with shear-forming strain. This effect was likely due to the increasing level of cold work as shear-forming strain increased. At high shear-forming strain levels, the axial strengths were comparable to 2195-T8 plate from the SLWT program, but the circumferential strengths were substantially less. The anisotropy increased with increasing shear-forming strain and was associated with increased texture intensity. The lower circumferential strength values for the shear formed cylinders compared with the 2195-T8 plate properties may have been due to slight differences in composition and an unoptimized thermomechanical processing schedule. The 2195 shear formed cylinders are a slightly different composition than the SLWT 2195 as shown in Table 1, and the heat treatment applied to the cylinders was developed for plate and sheet products and may not result in optimal mechanical properties when applied to shear formed products.

Elongation determined from fiducial mark analysis is plotted as a function of shear-forming strain in Figure 12 for the 2195-T8 cylinders. The data show that elongation varied inversely with shear-

forming strain as would be expected from the strength values. The ductilities exceeded 18% for all conditions. For the circumferential orientation, ductility ranged from 27% at the lowest level of shear-forming strain to 23% at the highest. The low circumferential strengths (compared with SLWT material) and the high ductility exhibited by the shear formed cylinders may indicate that the prescribed T8 heat treatment, derived for 2195 plate and sheet products, may need adjustment to optimize the strength/ductility combination for shear formed products.

4.2. C415 Shear Formed Cylinders

4.2.1. Microstructure. Triplanar images of the grain structure of C415-T3 cylinder 1 at the 0° position and depths of t/8 and 7t/8 are shown in Figure 13. The grain structure of cylinder 1 at 45° was very similar to the 0° position. Overall, C415-T3 cylinder 1 exhibited a recrystallized grain structure with clusters of fine grains interspersed with coarse grains. Isolated areas of fine grains were concentrated toward the outer half of the cylinder. Band-like rows of grains aligned approximately 45° to the axial direction were occasionally observed on the AC planes. In general, the grain structure became coarser and more elongated with increasing depth below the outer cylinder surface.

A through-thickness AR section from cylinder 6 (T3) is shown in Figure 14. The grain structure appeared to be recrystallized and non-uniform and exhibited a marked transition from a fine, equiaxed structure for approximately the outer half of the cylinder to a coarse, elongated structure for the inner half. The transition from fine to coarse grains occurred near midthickness. Cylinders 4 and 3, which had intermediate strain levels, had microstructures similar to cylinder 6. (Cylinder 5 was not characterized since it had the same processing history as cylinder 1.)

It was concluded that the microstructure seen in cylinder 6 evolved gradually from that of cylinder 1 as shear-forming strain increased due to grain refinement. The grain structure transition observed for cylinders 4, 3, and 6 probably resulted from refinement of the microstructure of the outer half of the cylinder due to concentration of deformation there during the mandrel shear forming process, and not from the application of some critical level of shear-forming strain to the material in general. During the subsequent solution heat treatment, the outer region of the cylinder would then be more prone to recrystallization, resulting in increased grain refinement in that area.

4.2.2 Texture. The objectives of the texture analysis included determination of the general texture characteristics and their uniformity and degree of symmetry through the thickness of the material. The effect of shear-forming strain on the texture and the correlation between the texture and the tensile properties were also to be determined.

Since deformation as well as recystallization components were observed, the discussion will focus on deformation fibers and individual recrystallization components. Overall, the texture of the C415 cylinders was weak, with maximum intensities less than six times random. The texture was independent of angular location (0° or 45° as shown in Figure 2). The overall texture varied through the thickness and was not symmetrical about the midplane.

The texture of cylinder 1 (ε=0.71) was extremely weak, as represented by the midthickness ODF shown in Figure 15. A deformation fiber-type texture developed as shear-forming strain increased to that of cylinder 6 (ε=1.88). For cylinder 6, the orientation and intensity of the deformation fiber were not constant through the thickness. The orientation and intensity of the fiber were also not symmetrical about the midplane. From near the outer surface (t/8, Figure 16) to the midthickness (t/2, Figure 17), the fiber was oriented between rolled (Bs) and cross-rolled (X-R) orientations as shown in Figures 16b and 17b, respectively. Near the inner surface (7t/8, Figure 18), the fiber was closer to a cross-rolled orientation. The definition and intensity of the deformation fiber was highest near the inner surface.

As seen from Figures 16b-18b, the Bs component was detected at all depths studied for cylinder 6, though some splitting of the intensity field is noted such that the concentrations straddled the ideal Bs orientation, indicated by the dot marked “Rolled (Bs)” in the figures. The angle of splitting increased

from 0° at t/8, to 14° and 18° at t/2 and 7t/8, respectively. This angle represents rotation about the axial direction of the cylinder. Since this data was obtained prior to flattening the cylinders, the texture was sampled on a planar section through the curved cylinder wall, causing an apparent splitting of the intensity fields about the ideal Bs location. The increase in the angle of splitting from t/8 (near the outer surface) to 7t/8 (near the inner surface) is likely due to the increasing radius of curvature of the cylinder wall as it is traversed from the outer to the inner surfaces.

As mentioned, some recrystallization components were observed for the C415 cylinders, notably Cube and various Rotated Cube components (RC_{RD} or RC_{TD}). These components are indicated for cylinder 6 at t/8, t/2, and 7t/8 in Figure 19. (The corresponding complete ODF's and deformation fibers were shown in Figures 16-18.) A weak Cube component can also be seen for cylinder 1 in Figure 15 as concentrated intensity in the corners of the ϕ_2=0 section at the upper left of the figure.

The flattening procedure did not significantly alter the texture. The weakness of the texture for the C415 cylinders correlates well with the relatively isotropic yield strength. (The yield strengths are shown in Table 7 and will be discussed in the next section.)

4.2.3. Mechanical properties. An overview of the tensile behavior of both the direct-aged and reprocessed C415-T8 shear-formed cylinders is shown in Tables 7 and 8. Data is presented for both the axial (A) and circumferential (C) orientations. Table 7 also includes data for C415-T8 0.090-in.-thick sheet in the longitudinal (L) and transverse (T) orientations for comparison [23]. Figures 20 a) and b) show the effect of shear-forming strain on yield strength (YS) and ultimate tensile strength (UTS) for the direct-aged and reprocessed cylinders, respectively. In both figures, average yield and ultimate strengths for the C415-T8 sheet are shown as dotted lines for comparison.

Table 7 shows that the elastic modulus remained nearly constant regardless of aging procedure, level of shear-forming strain, or specimen orientation. It can also be seen that overall, the direct-aged T8 material had higher yield and tensile strengths than the reprocessed material. This effect was generally seen regardless of the level of shear-forming strain or specimen orientation, although it was most pronounced for the axial specimen orientation at lower shear-forming strain.

For the direct-aged material (Figure 20a), axial strengths exceeded the corresponding circumferential strengths, while the opposite trend was seen for the reprocessed material (Figure 20b). The level of anisotropy was generally less than 3%, which would be expected given the weak texture. In general, the yield and ultimate strengths decreased slightly with increasing shear-forming strain for both material conditions. Yield and ultimate strengths for all material conditions and orientations tested were within 5% of the values for C415 sheet.

The ductility as indicated by the extensometers exceeded the 15% operating strain range for cylinder 1 in both the direct-aged and reprocessed conditions. The fiducial marks analysis (of only one sample per condition) indicated ~27% elongation for the axial orientation for both the direct-aged and reprocessed conditions, and 21-23% for the circumferential orientations.

Data for cylinder 6 from both the extensometers and fiducial marks indicated extensions of approximately 10-11% for the direct-aged material and ~13-16% for the reprocessed material, with axial ductility normally exceeding circumferential ductility. Comparing cylinders 1 and 6, the elongation showed a significant decrease with increasing level of shear-forming strain, as seen in Table 8 and Figure 21.

Table 7. Tensile Properties for C415-T8 Shear Formed Cylinders and 0.090-inch Sheet.

			E (Msi)		Yield Strength (ksi)		Ultimate Strength (ksi)	
Cylinder	ε	Orien-tation.	Direct Aged	Reprocessed	Direct Aged	Reprocessed	Direct Aged	Reprocessed
1	0.71	A	10.7	10.5	75.1	69.2	80.7	77.1
		C	10.5	10.6	73.9	73.2	80.1	78.7
6	1.88	A	10.3	10.4	73.8	70.2	76.1	76.8
		C	10.5	10.2	71.7	72.1	77.6	76.8
Sheet [23]		L	-	-	73.3		78.6	
		T	-	-	70.8		77.2	

Table 8. Ductility for C415-T8 Shear Formed Cylinders.

			% Elongation (0.3-in. Extensometers)		% Elongation (0.5-in. Fiducial Marks)	
Cylinder	ε	Orien-tation.	Direct Aged	Reprocessed	Direct Aged	Reprocessed
1	0.71	A	>15	>15	27.8	27.1
		C	>15	>15	20.7	23.4
6	1.88	A	no data	12.9	11.8	16.5
		C	9.5	14.4	11.3	14.5

Complete K-R curves are shown in Figure 22 for the duplicate CT specimens from cylinder 1 tested in each condition. Higher overall toughness was achieved for material in the reprocessed condition, as evidenced by the higher K-R curves, compared with direct-aged material. The divergence observed in the K-R curves for the reprocessed material is likely due to crack path variations. In all specimens tested, a fully slant fracture (either single or double shear lips) developed after about 0.15 inches of physical crack extension. When a single shear lip occurred the crack advanced nominally along the specimen centerline (i.e., in the circumferential direction for the AC specimen). However, when double shear lips developed, crack turning was observed and crack growth moved toward the axial direction. The lower curve is associated with crack growth in the circumferential direction, and the higher curve is associated with crack turning. Crack turning occurred in both of the direct-aged specimens. The crack growth resistance parameter, $K_{0.15}$, was selected because after 0.15 inches of physical crack extension the crack front was in fully plane stress conditions in all specimens.

A summary of fracture toughness values is provided in Table 9 for both material conditions. Values for initiation toughness, K_{JIc}, agreed within 5% for both the direct-aged and reprocessed material. However, crack growth resistance, as indicated by $K_{0.15}$, was higher on average by about 20% for the reprocessed material, which was consistent with the trend of lower yield strength for that condition.

Table 9. Fracture Toughness Values for C415 Cylinder 1.

Condition	Specimen	K_{JIc}	$K_{0.15in}$
Direct-Aged	1	33.7	76.8
	2	34.1	77.7
	Avg.	33.9	77.3
Reprocessed	1	32.3	81.4
	2	39.0	95.2
	Avg.	35.7	88.3

5. Conclusions

- The deformation process during shear forming can best be described as a mixture of rolling and extrusion. This work revealed that texture characteristics were most readily interpreted when the axial direction was assumed to be the principal deformation axis. The reference direction is significant in that it is perpendicular to the actual rolling direction.

The remaining conclusions are best presented by separating the 2195 and C415 results:

- The microstructure of the 2195 shear formed cylinders produced by the counter-roller method was partially recrystallized. It consisted of elongated recrystallized grains interspersed with areas of high substructure content and deformation bands. The grain size became more refined and increasingly inhomogeneous with increasing shear-forming strain. The through-thickness microstructural gradients suggest that deformation was concentrated at the inner surface of the cylinders during the shear forming process.

- The texture of the 2195 shear formed cylinders was dominated by a rolling-type deformation fiber, which varied in intensity both through-thickness and with increasing shear forming strain. The orientation of the fiber also varied through-thickness, transitioning from a β-type fiber (near the outer surface), to a cross-rolled fiber (at the mid-plane) and finally to an orientation close to an extrusion fiber (near the inner surface). The intensity of the fiber increased with increasing shear-forming strain and from the outer surface inward.

- The tensile properties of the 2195-T8 shear formed cylinders were lower than the typical values reported for SLWT 2195-T8 plate materials. The tensile strengths increased and ductility decreased with increasing shear forming strain. The yield strength was anisotropic, being higher in the axial than the circumferential direction. In combination with the texture data, this is consistent with the mechanical behavior of 2195 rolled product and thick-section extrusions. Yield strength anisotropy was also observed to increase with shear-forming strain.

- The microstructure of the C415 shear formed cylinders produced by the mandrel method was mostly recrystallized. For low levels of shear-forming strain, the grain structure was homogeneous through-thickness. However, as the shear-forming strain increased, the grain structure developed into a fine-grained layer between the midthickness and the outer surface, and a coarse-grained layer between the midthickness and the inner surface. The layered effect was attributed to extensive grain refinement in the outer region caused by a concentration of deformation there. Deformation was concentrated in the outer region due to the application of the roller to the outer surface.

- The texture of the C415 shear formed cylinders exhibited a rolling-type deformation fiber which varied in orientation from a β-type rolling fiber near the outer surface, to a cross-rolled fiber near the inner surface for high levels of shear-forming strain. The fiber was between rolled and cross-rolled orientations at the midthickness. The fiber was most intense and well-defined near the inner surface. Some recrystallization texture was also observed, mainly Cube and various Rotated Cube components.

- The tensile strengths of the C415 shear formed cylinders were fairly isotropic, consistent with the weak texture. The tensile strengths were relatively insensitive to shear-forming strain level or T8 procedure (direct-aged or reprocessed) and compared favorably with 0.090-inch-thick C415-T8 sheet for all conditions. The ductility was relatively constant with T8 procedure but decreased with increasing shear-forming strain. Initiation toughness was not sensitive to T8 procedure, but crack growth resistance was higher for the reprocessed material.

Acknowledgements

This work was performed while the author, Lillianne P. Troeger, held a National Research Council/NASA-LaRC Research Associateship. The authors would like to thank Dr. Stephen Hales of NASA LaRC for many helpful discussions.

References

[1] Enright, E.; and Hartley, P.J.: Aluminum-Lithium Technology for Launch Vehicles. Martin Marietta IR&D M-40-D. Final Report, 1994.

[2] Eckert, M.; and Schmeer, E.: Production of Motor Casings by Shear Forming. *Proceedings of the. 32nd Mechanical Working and Steel Processing Conference*, vol. 28, 1990, pp. 297-305.

[3] Furrer, David; and Noel, Robert: Aluminum-Lithium Cylinders. *Advanced Materials and Processes*, vol. 151, no. 5, 1997, pp. 59-60.

[4] Reinmuller, R.E.: Report on Allowables for 2195 Used for the Shuttle External Tank. Presented at *AeroMat '97*, 1997.

[5] Lockheed Martin-Manned Space Systems: *Al-Li Materials Database*. Service Order SO-96-89818, 1996A.

[6] Aluminum Association: *Registration Record of International Alloy Designations and Chemical Composition Limits for Wrought Aluminum and Wrought Aluminum Alloys*, 1998.

[7] Lederich, R.J.; Sastry, S.M.L.; Hayase, M.; Mackay, T.L.: Superplastic Formability Testing. *Journal of Metals*, 1982, pp. 16-20.

[8] Goforth, R.E.; Chandra, N.A.; and George, Dorsey: Analysis of the Cone Test to Evaluate Superplastic Forming Characteristics of Sheet Metal. *Superplasticity in Aerospace* (TMS), 1988, pp. 149-166.

[9] Safiullin, R.V.; and Enikeev, F.U.: Determination of Thinning Characteristics During Sheet Forming Processes. *Superplasticity and Superplastic Forming*, (TMS: Warrendale, PA), 1995, pp. 213-217.

[10] *Aluminum and Aluminum Alloys*: ASM Specialty Handbook, ASM International (Materials Park, OH: 1993), p. 30

[11] Domack, M.S.; Dicus, D.L.; Edahl, R.A.; and Chellman, D.J.: Effect of Thermal Exposure on the Strength-Toughness Behavior of Elevated Temperature Service Aluminum Alloys. *Proceedings of the Sixth International Conference on Aluminum Alloys*, vol. 2, 1998, pp. 1081-1086.

[12] Lockheed Martin Manned Space Systems: Engineering Material Specification STM 11A1-2, (revised 1/22/96) 1996B.

[13] Starke, E.A., Jr.: NASA-UVA Light Aerospace Alloy and Structures Technology Program Supplement: Aluminum-Based Materials for High Speed Aircraft. NASA CR-97-206248, 1997, pp. 3-51.

[14] Doherty, Roger D.: Recrystallization and Texture. *Progress in Materials Science*, v. 42, 1997, pp. 39-58.

[15] "Standard Test Method for Tension Testing of Metallic Material," *1999 Annual Book of ASTM Standards*, vol. 03.01, 1999, p. 57.

[16] "Standard Test Method for Determining J-R Curves," *1995 Annual Book of ASTM Standards*, vol. 03.01, 1995, p. 763.

[17] Anderson, T.L.: *Fracture Mechanics: Fundamentals and Applications (CRC Press* CRC: Boston, MA), 1991, p. 446.

[18] "Standard Test Method for J_{Ic}, A Measure of Fracture Toughness," *1995 Annual Book of ASTM Standards*, vol. 03.01, 1995, p. 646.

[19] Bunge, H.J.: Three-Dimensional Texture Analysis. *International Materials Reviews*, vol. 32, no. 6, 1987, pp. 265-291.

[20] Cahn, Robert W., ed.: *Processing of Metals and Alloys. Materials Science and Technology: A Comprehensive Treatment*, vol. 15 (VCH) 1991, pp. 429-480.
[21] Fricke, W.G., Jr. and Przystupa, M.A: Texture in *Aluminum Alloys- Contemporary Research and Applications. Treatise on Materials Science and Technology vol. 31 (Academic Press: London)* 1989.
[22] Hales, S.J.; and Hafley, R.A.: Texture and Anisotropy in Al-Li Alloy 2195 Plate and Near-Net-Shape Extrusions. *J. Materials Science and Engineering*, vol. 257A, no. 1, 1998, pp. 154-165.
[23] Chellman, David; Cornell, Brian; Bayha, Thomas; and West, Jacquelyne: Aluminum Alloy Development: HSR Airframe Technology-Metallic Materials. Final Report. Lockheed Martin Aeronautical Systems LG97ER0037, 1997, p. 71.

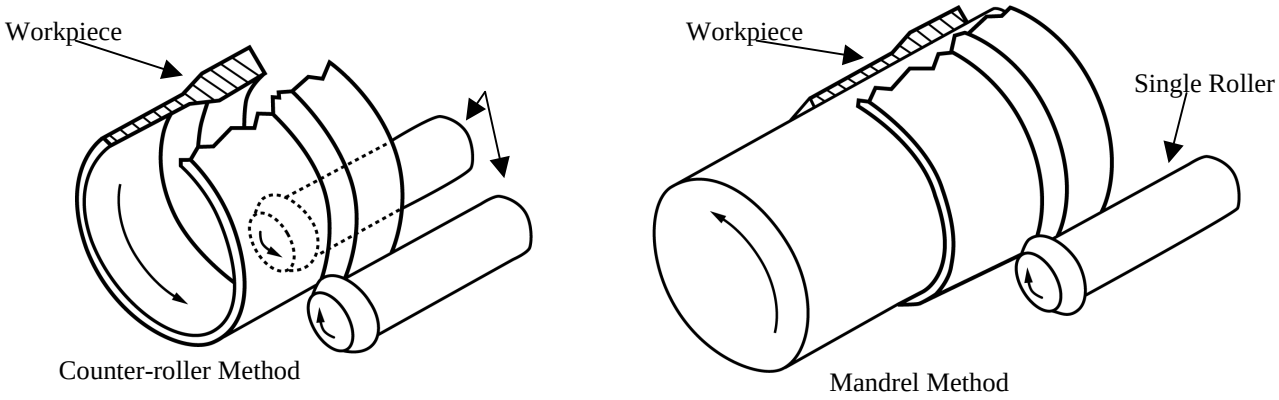

Figure 1. Diagram of shear forming processes [3].

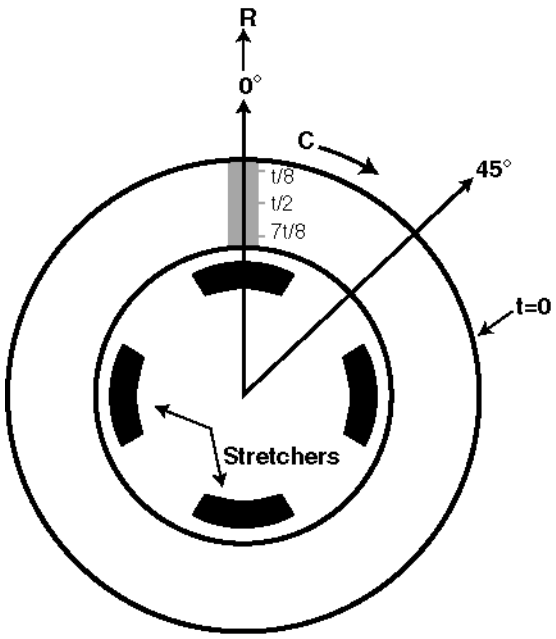

Figure 2. Depth locations for shear formed cylinders. In addition, angular locations are shown relative to final stretcher positions; these apply to C415 cylinders only.

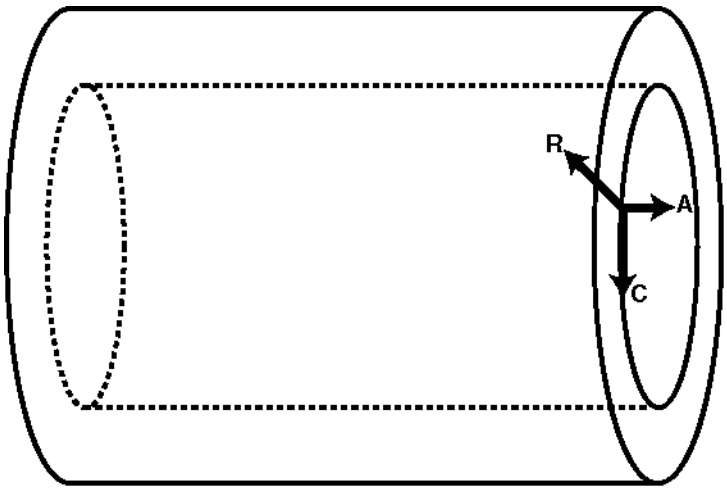

Figure 3. Cylinder coordinate system showing (A)xial, (R)adial, and (C)ircumferential axes.

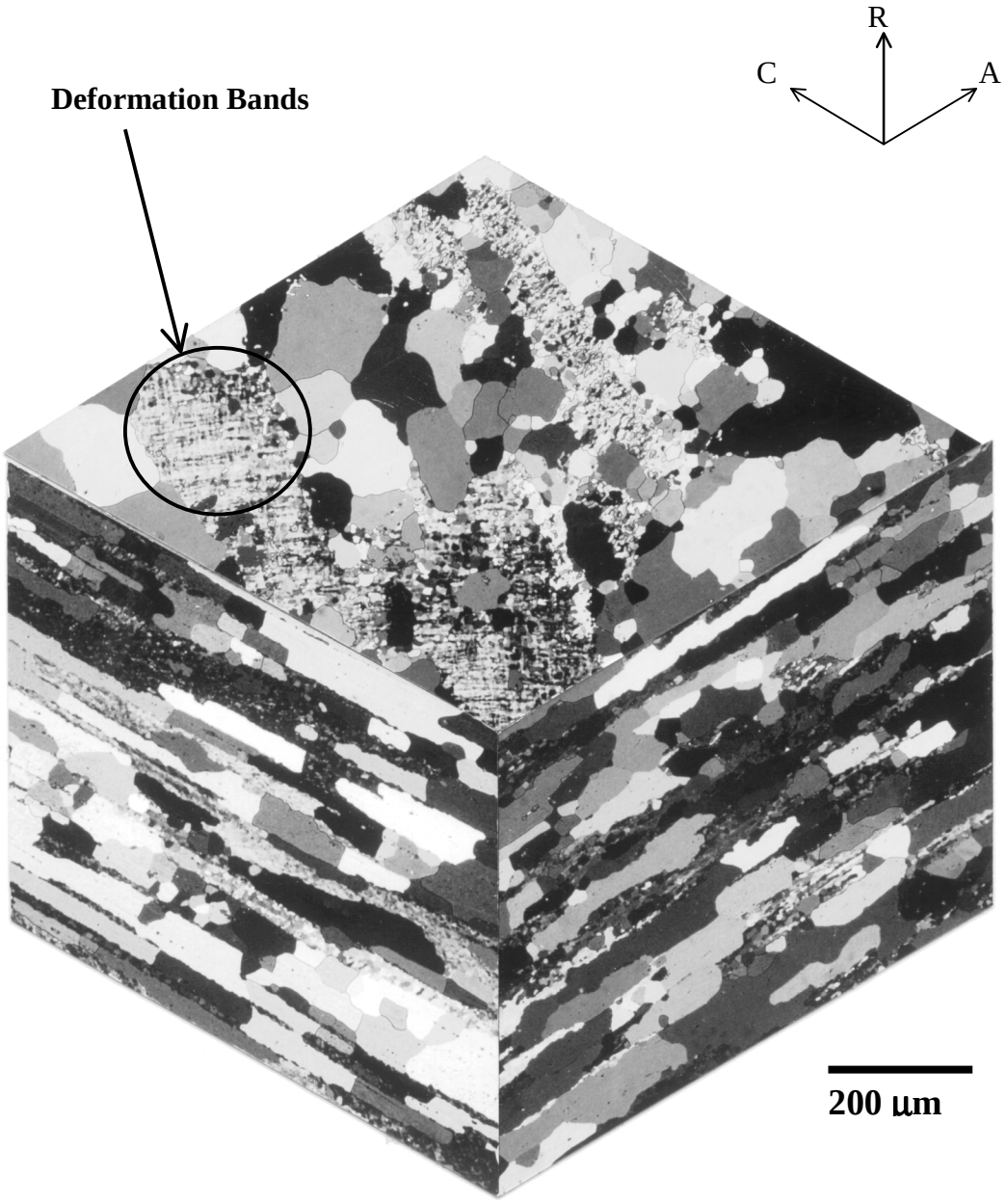

Figure 4. 2195-T4 shear formed cylinder D (ε=0.69) at midthickness.

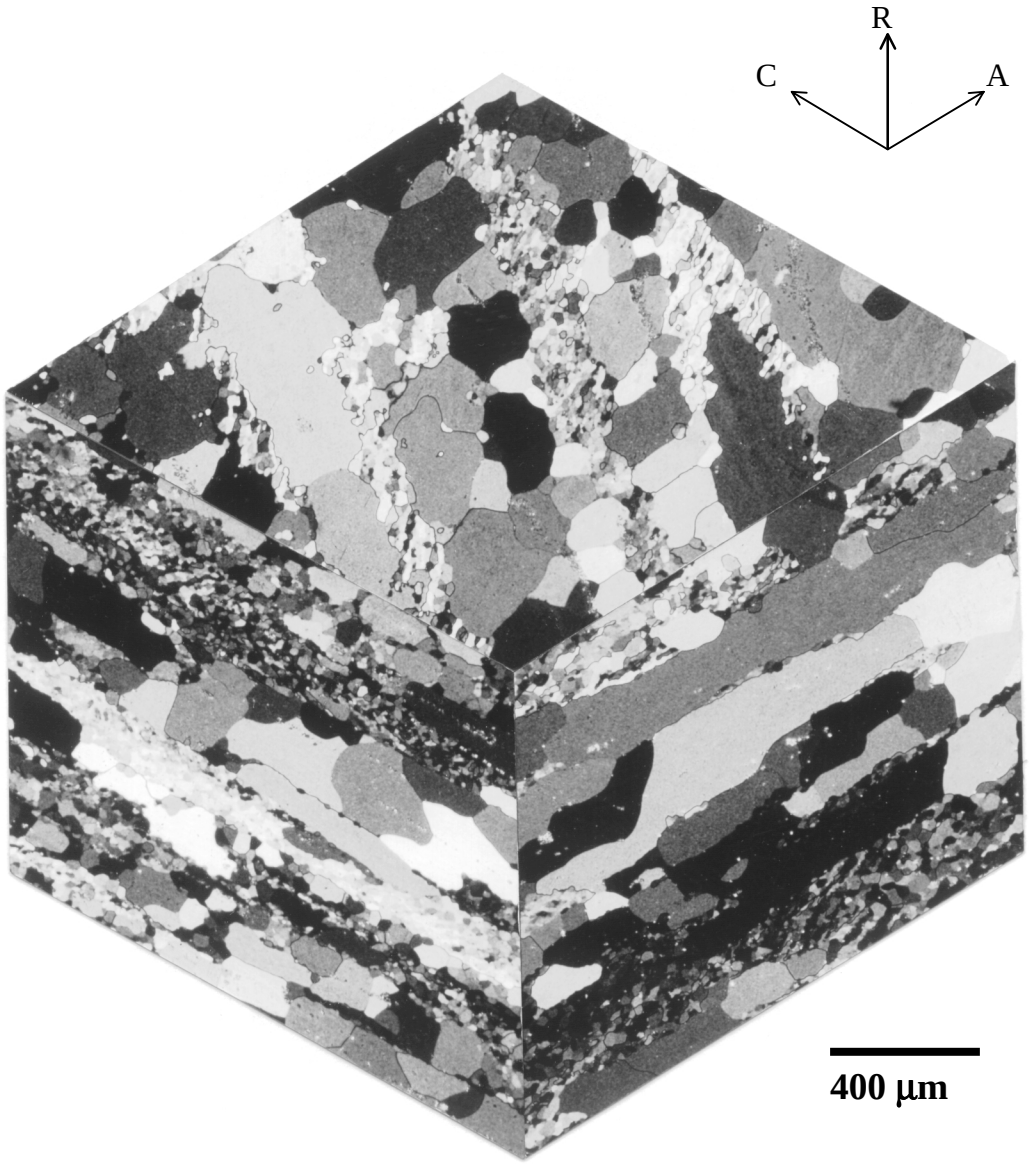

Figure 5. 2195-T4 shear formed cylinder D (ε=0.69) at t/8.

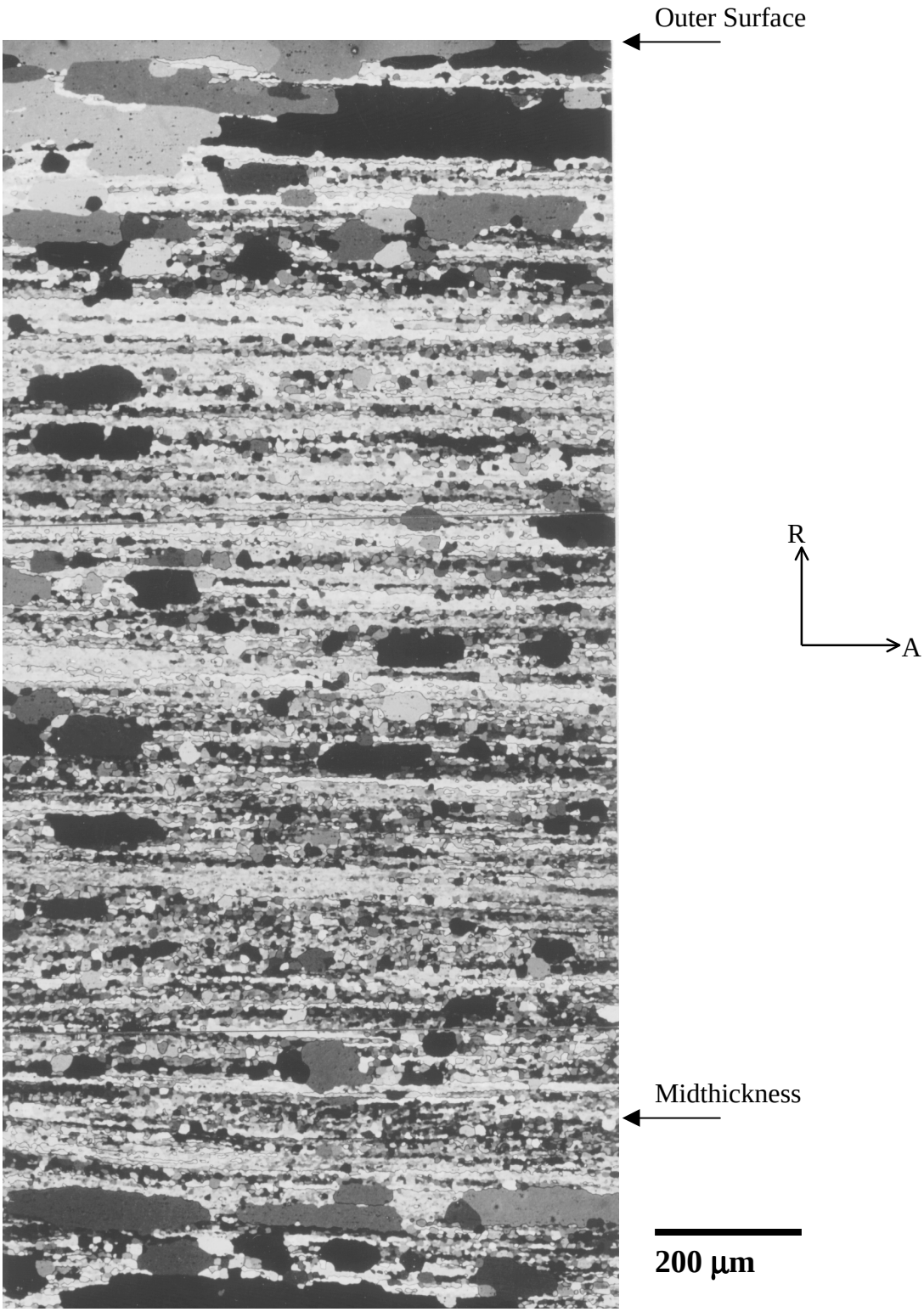

Figure 6a. 2195-T4 shear formed cylinder C (ε=1.61) from outer diameter (top) to midthickness (near bottom).

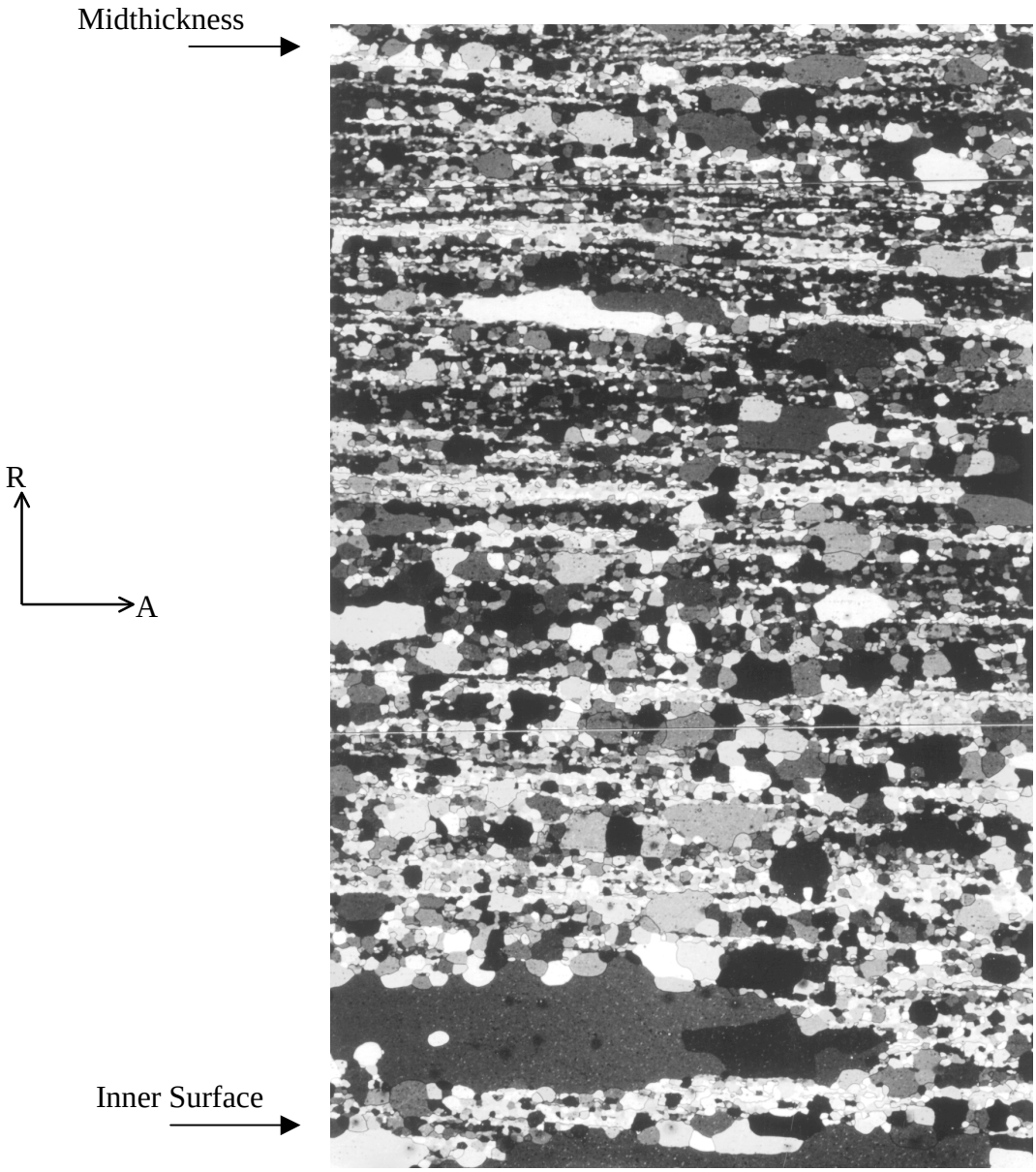

Figure 6b. 2195-T4 shear formed cylinder C (ε=1.61) from midthickness (top) to inner diameter (bottom).

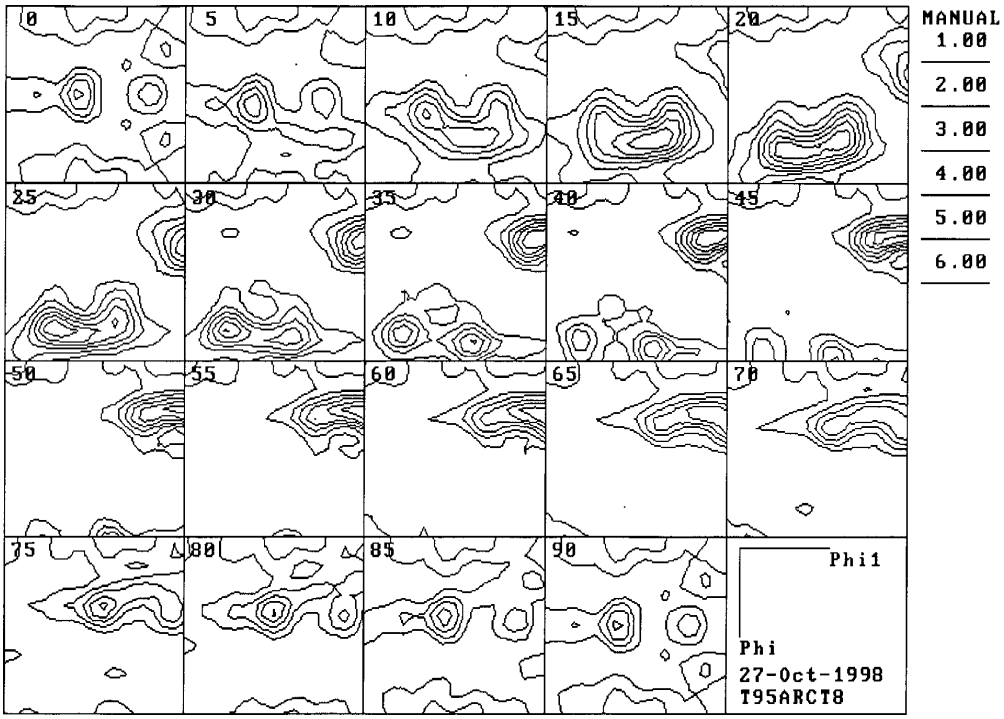

a) Complete ODF

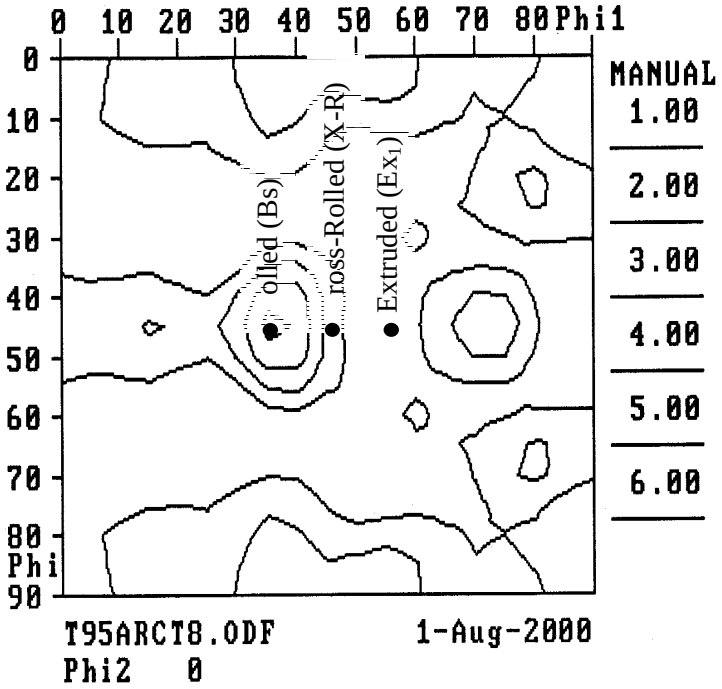

b) ϕ_2=0 section

Figure 7. ODF for 2195-T4 cylinder C (ε=1.61) at t/8.

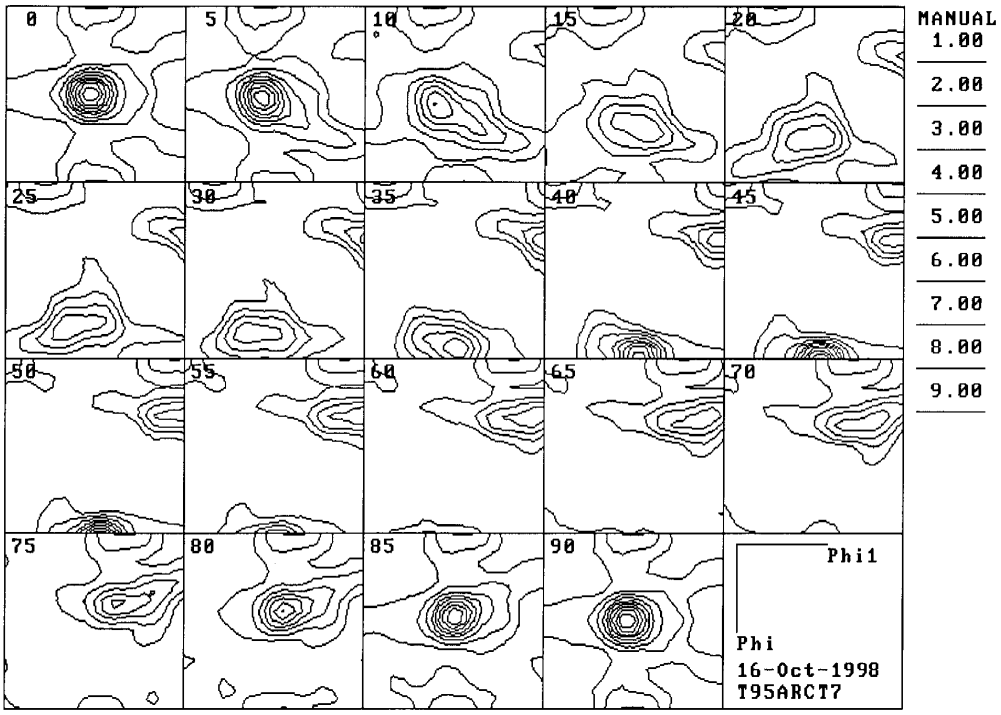

a) Complete ODF

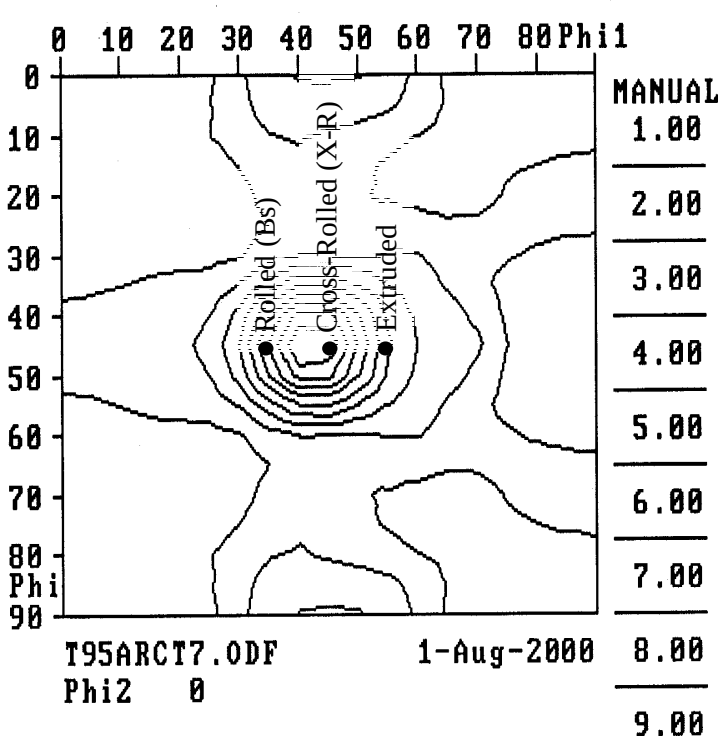

b) ϕ_2=0 section

Figure 8. ODF for 2195-T4 cylinder C (ε=1.61) at 7t/8.

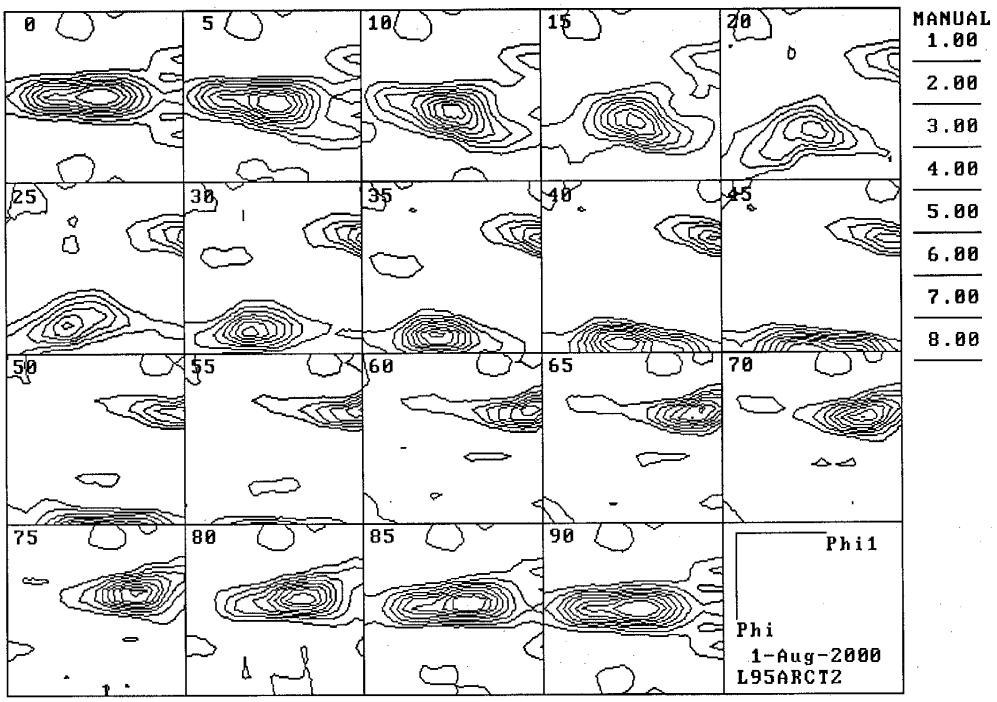

a) Complete ODF

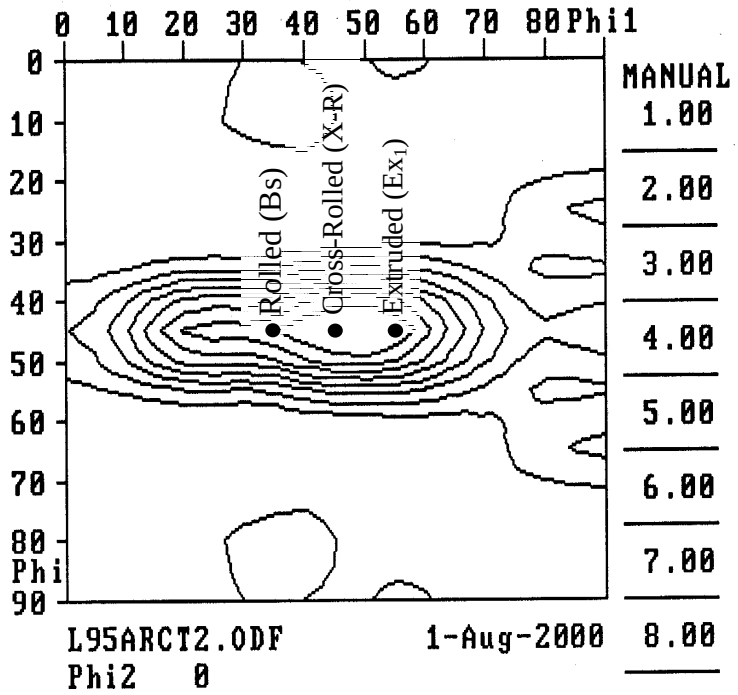

b) ϕ_2=0 section

Figure 9. ODF for 2195-T4 cylinder C (ε=1.61) at t/2

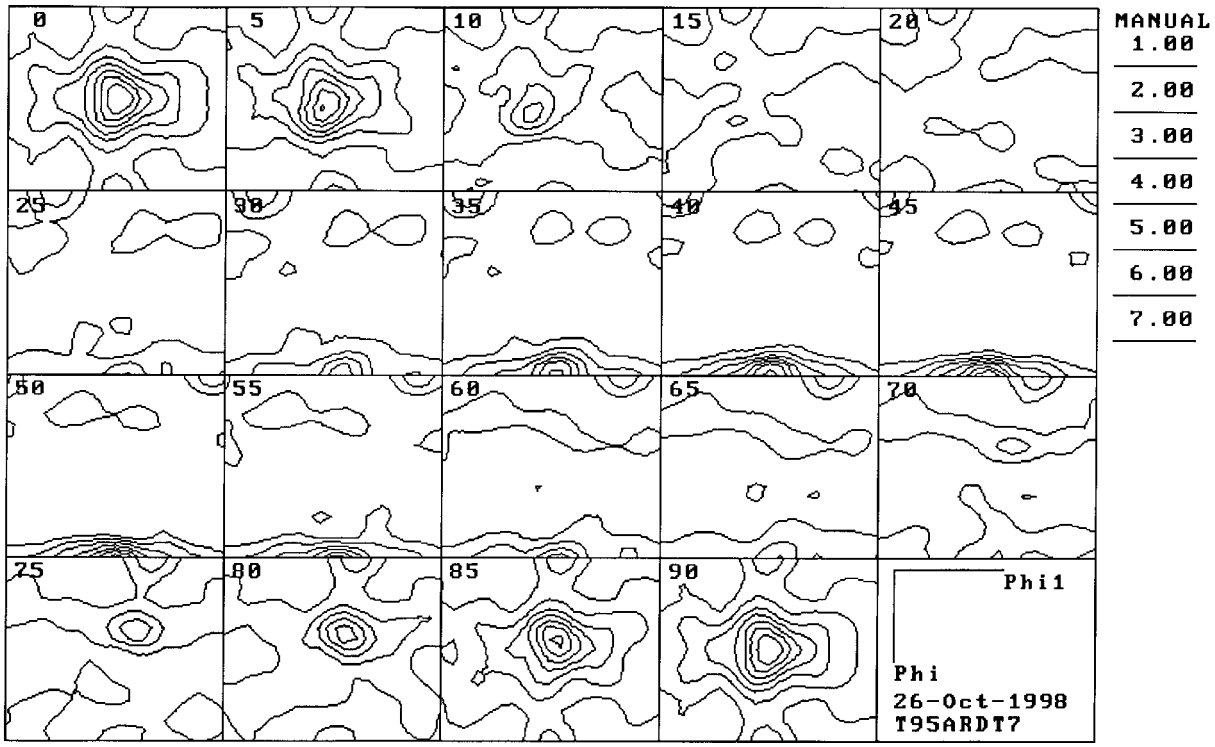

Figure 10. ODF for 2195-T4 cylinder D (ε=0.69) at 7t/8.

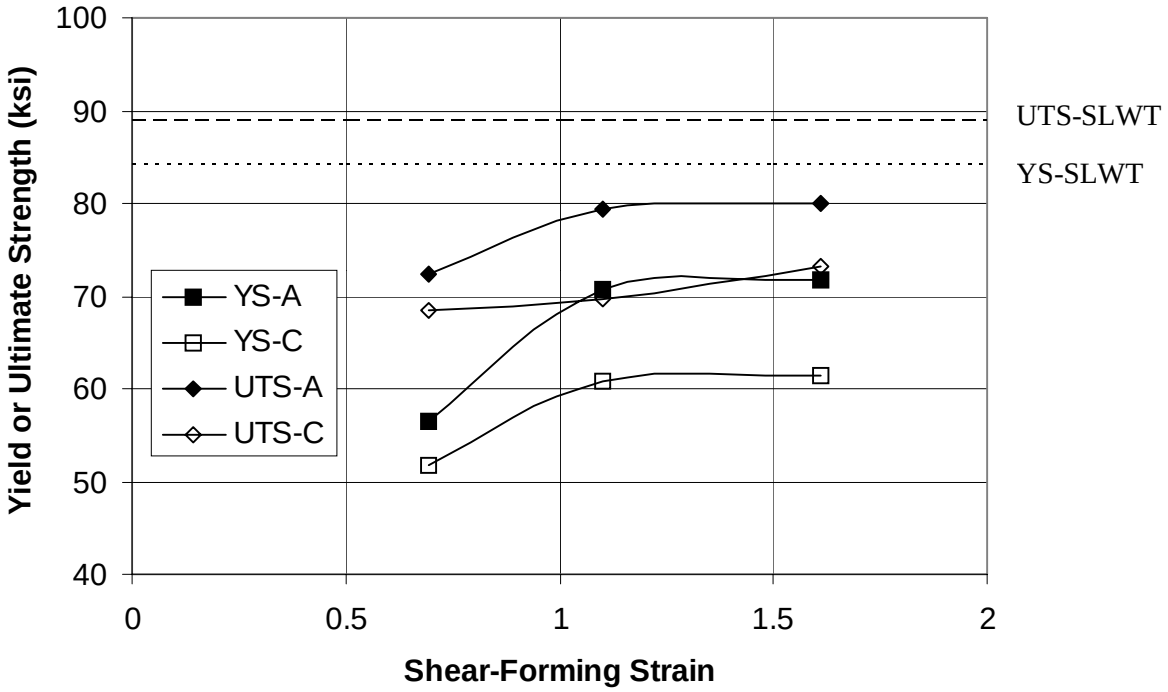

Figure 11. Effect of shear-forming strain on yield strength (YS) and ultimate tensile strength (UTS) for the 2195-T8 shear formed cylinders in both the axial (A) and circumferential (C) orientations, compared with typical values for 2195-T8 SLWT plate [5].

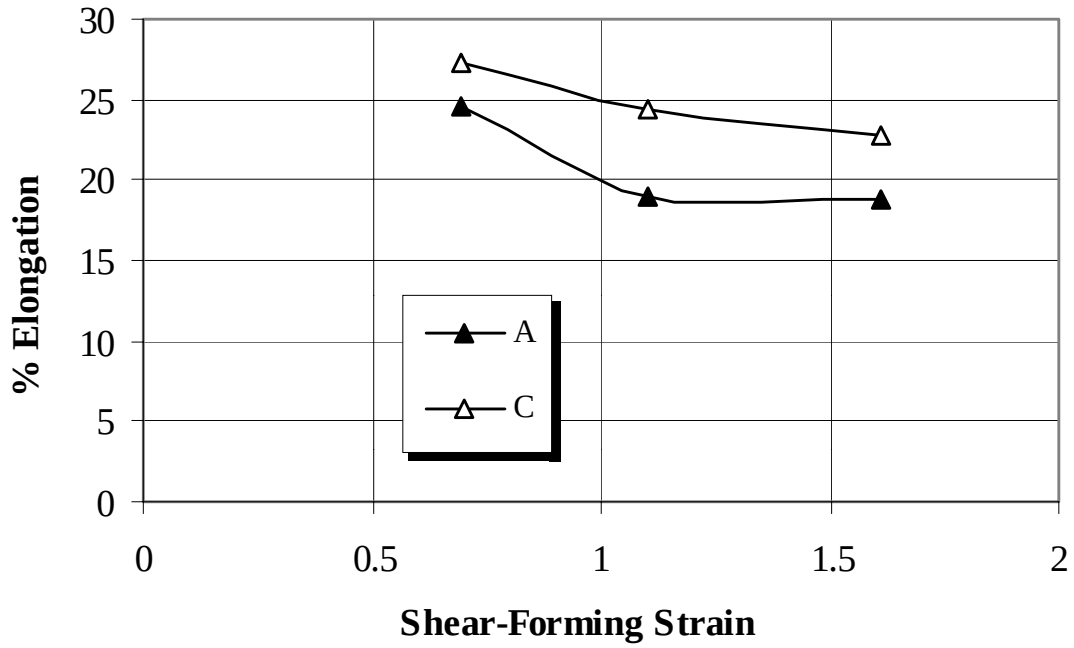

Figure 12. Effect of shear-forming strain on room-temperature ductility for the 2195-T8 shear formed cylinders in both the axial (A) and circumferential (C) orientations.

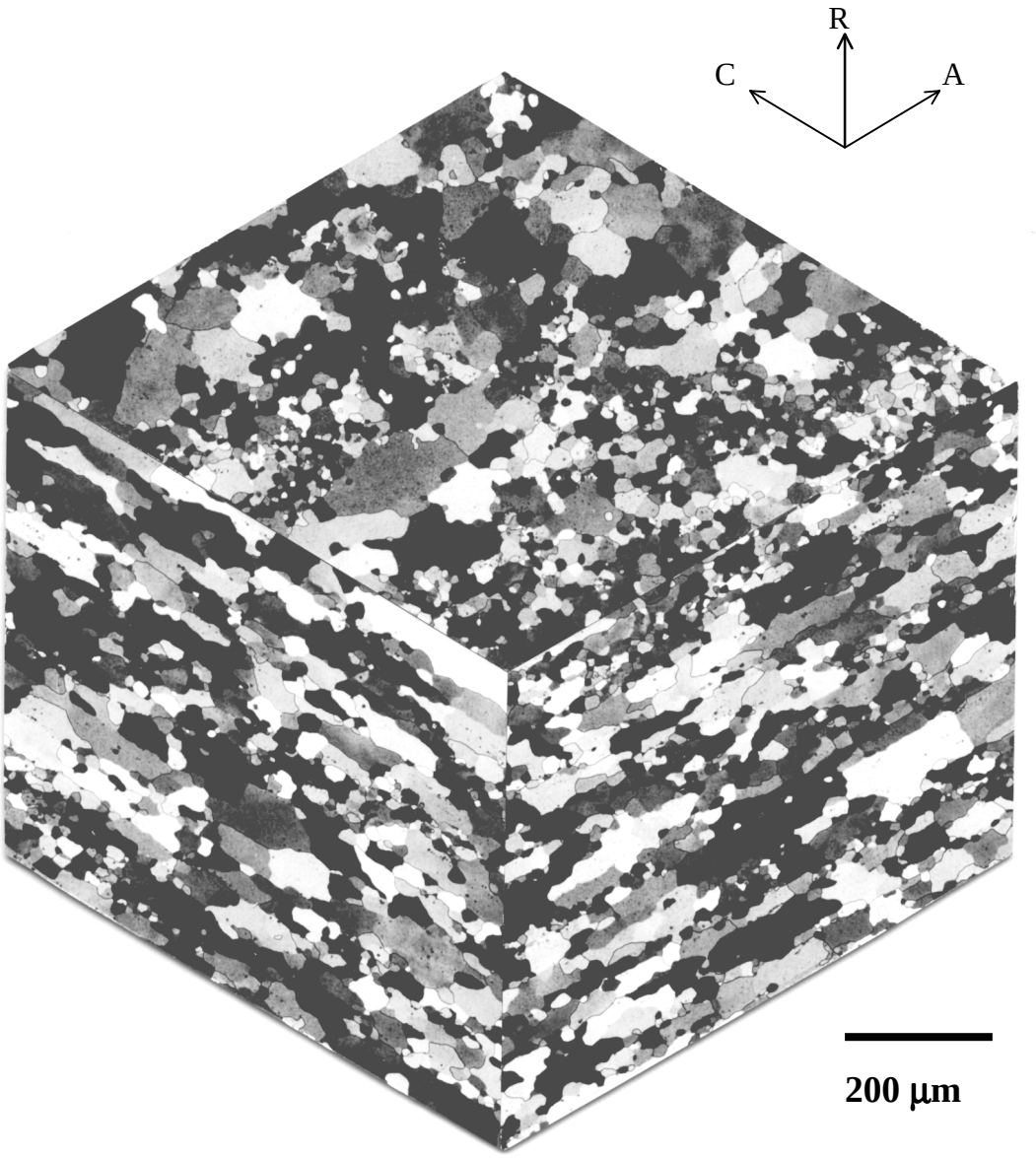

a) t/8

Figure 13. C415-T3 shear formed cylinder 1 (ε=0.72) at 0°.

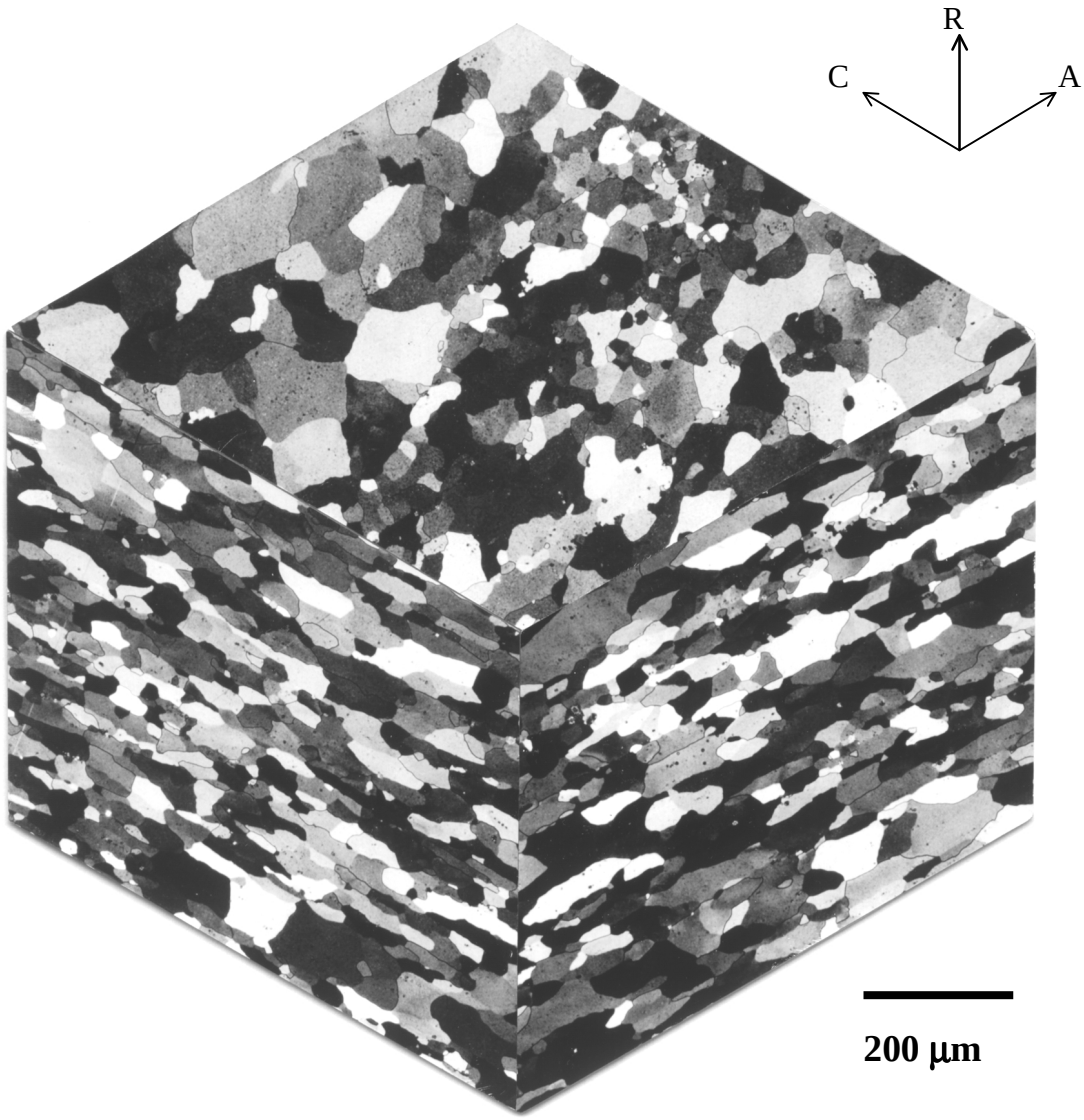

b) 7t/8

Figure 13. C415-T3 shear formed cylinder 1 (ε=0.72) at 0° (continued).

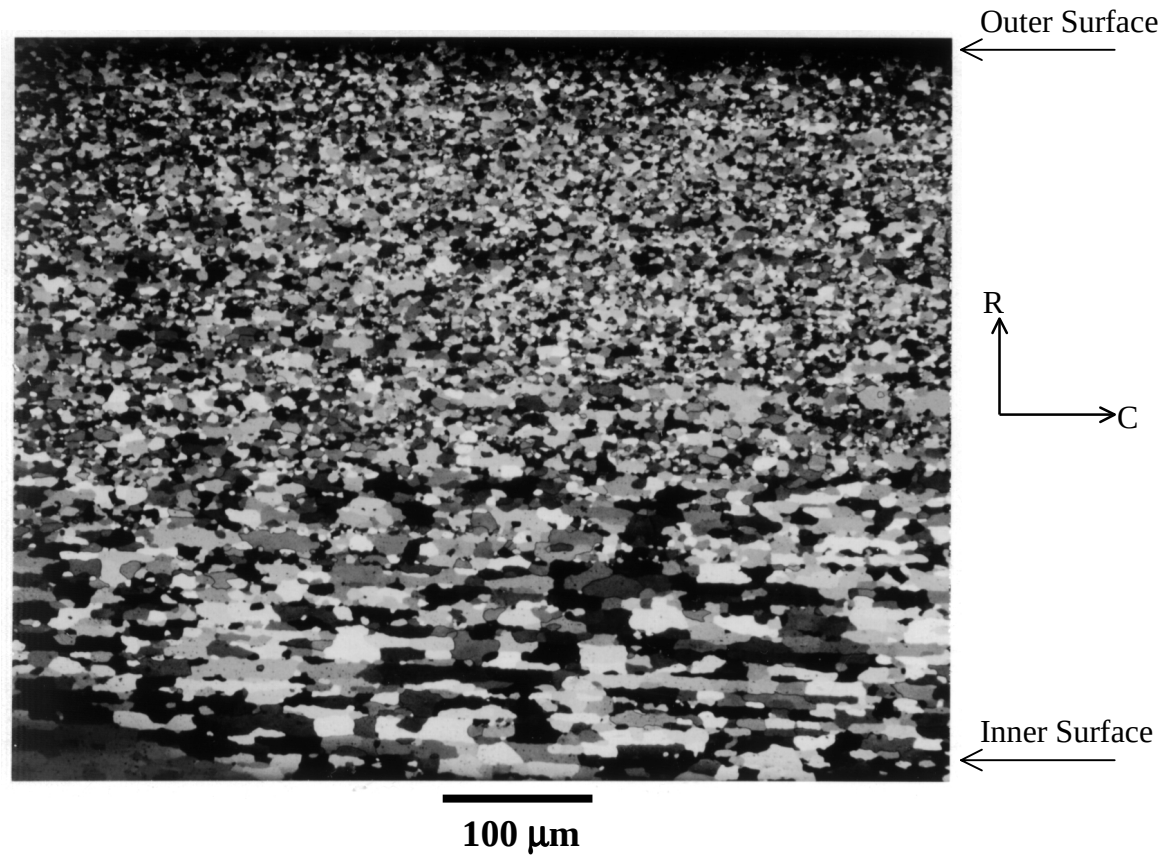

Figure 14. C415-T3 shear formed cylinder 6 (ε=1.88) at 0°, encompassing a full-thickness RC plane.

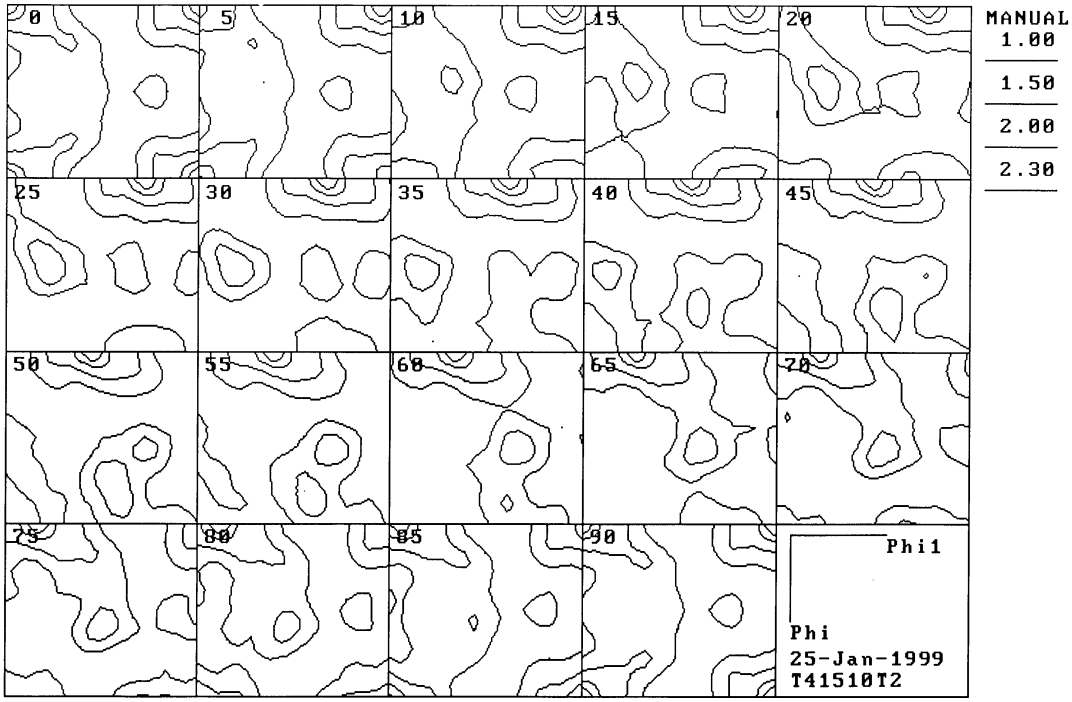

Figure 15. ODF for C415-T3 shear formed cylinder 1 at t/2 (0°).

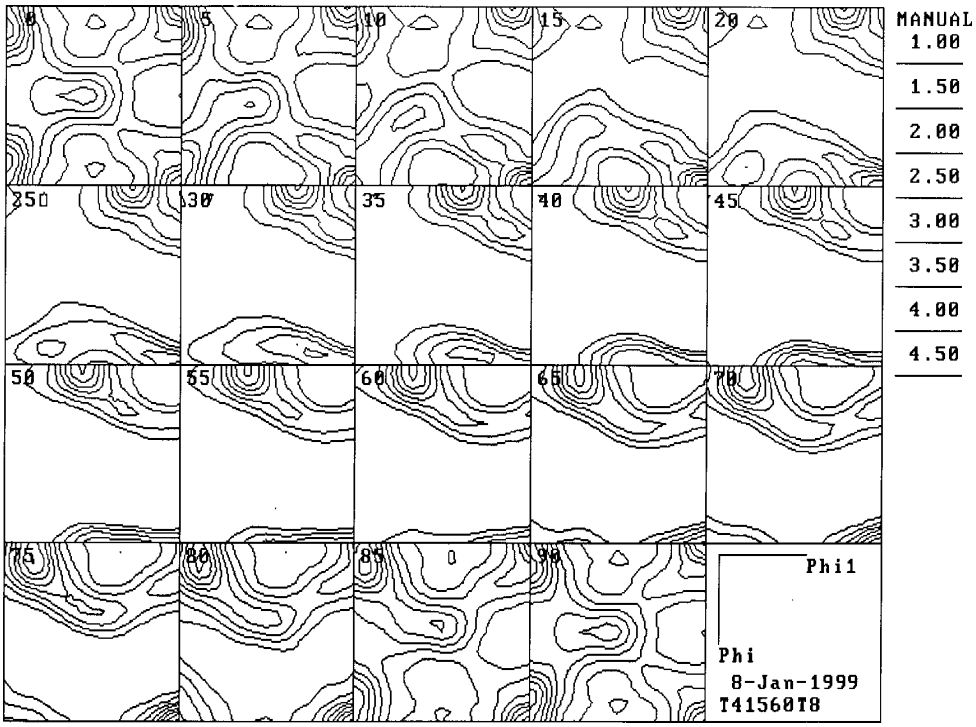

a) Complete ODF

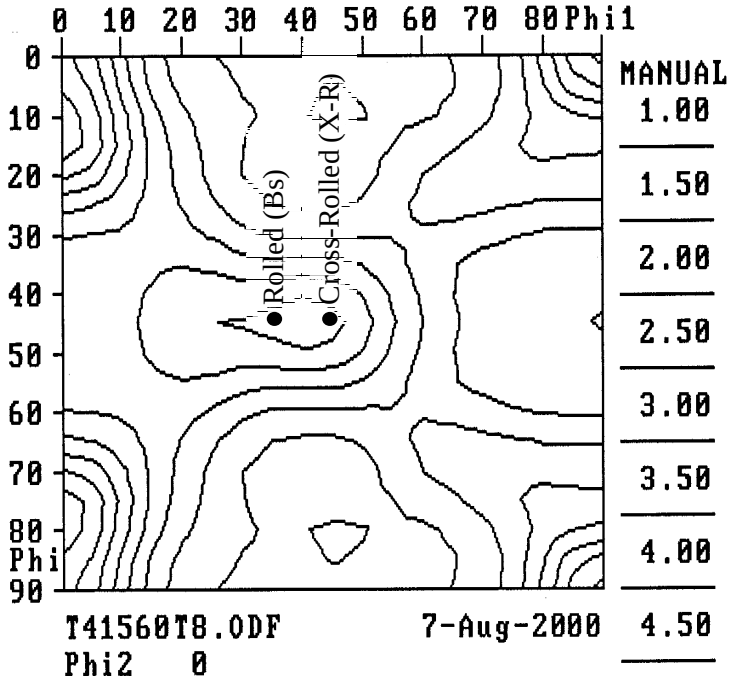

b) ϕ_2=0 section

Figure 16. ODF for C415-T3 shear formed cylinder 6 (ε=1.88) at t/8.

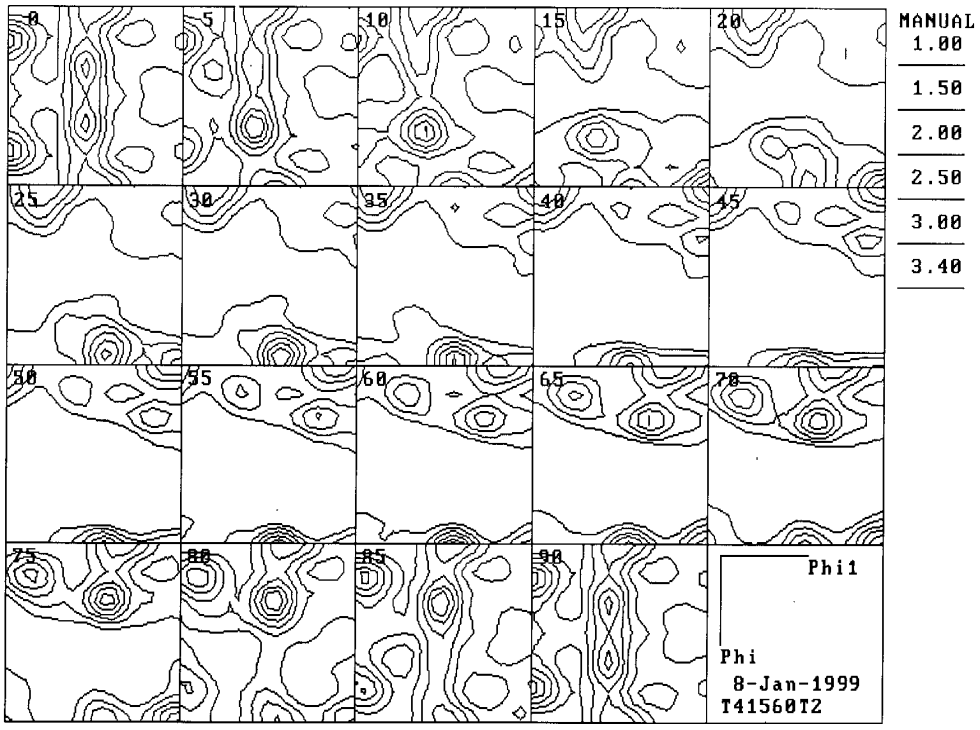

a) Complete ODF

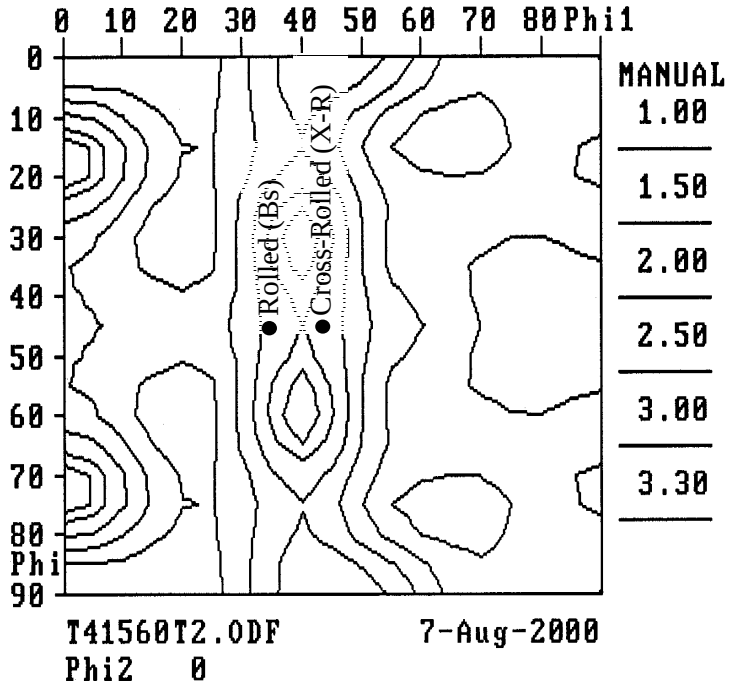

b) ϕ_2=0 section

Figure 17. ODF for C415-T3 shear formed cylinder 6 (ε=1.88) at t/2.

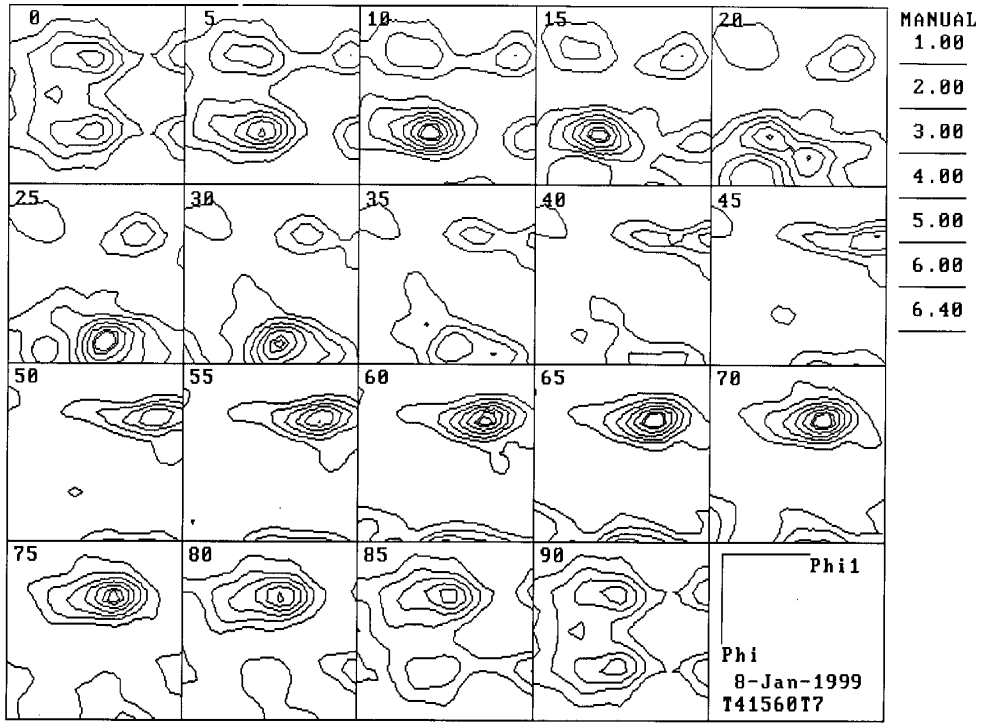

a) Complete ODF

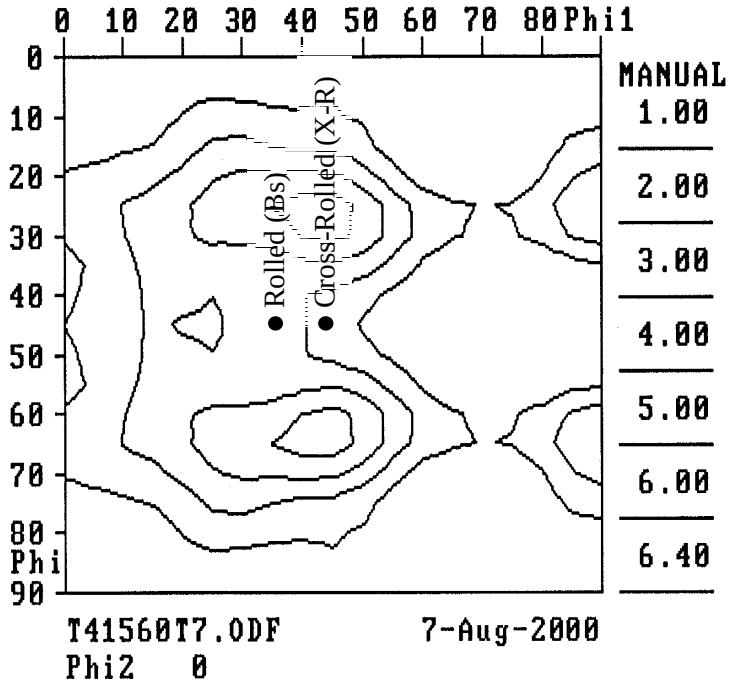

b) ϕ_2=0 section

Figure 18. ODF for C415-T3 shear formed cylinder 6 (ε=1.88) at 7t/8.

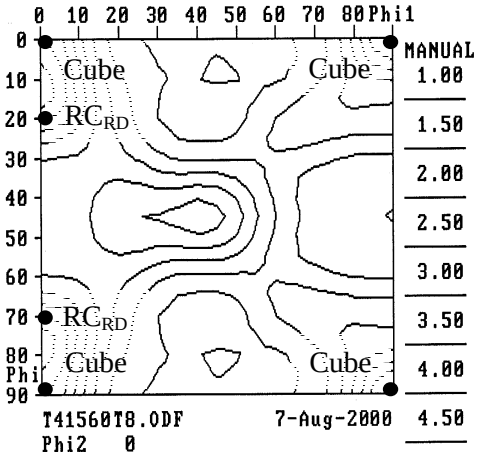

a) t/8

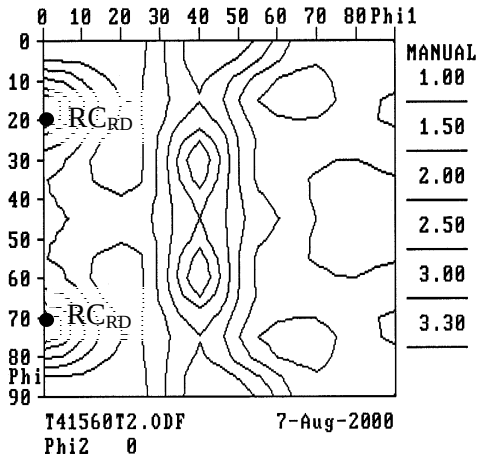

b) t/2

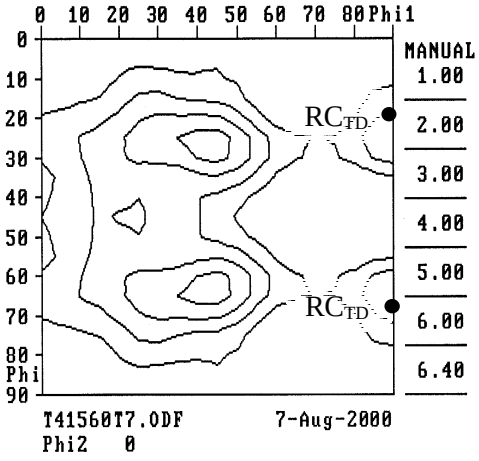

c) 7t/8

Figure 19. ϕ_2=0 sections for C415-T3 shear formed cylinder 6 (ε=1.88).

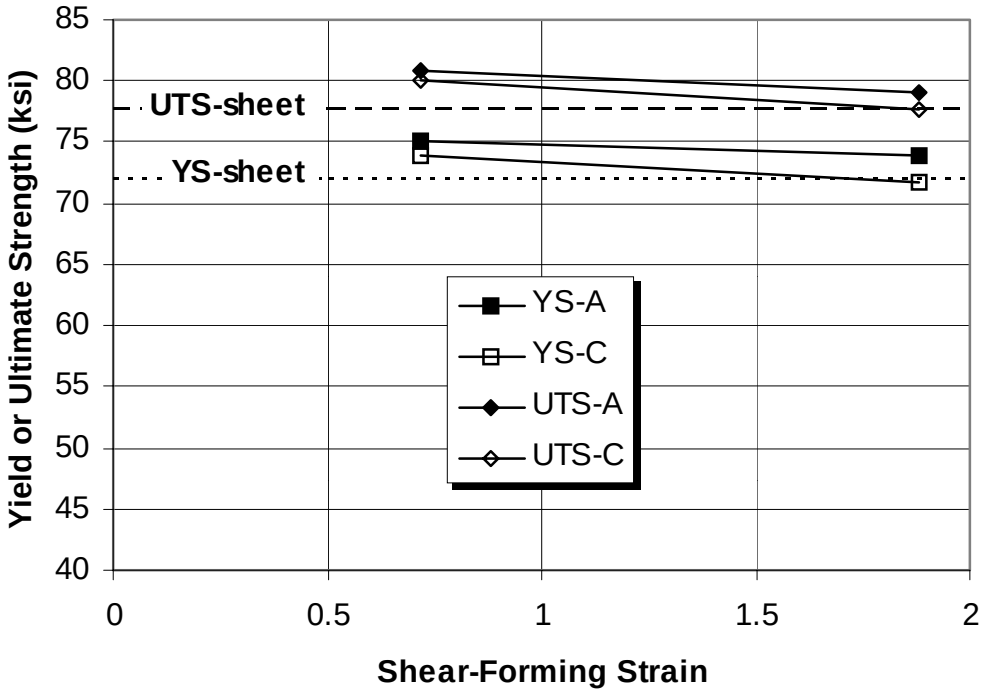

a) Direct-aged

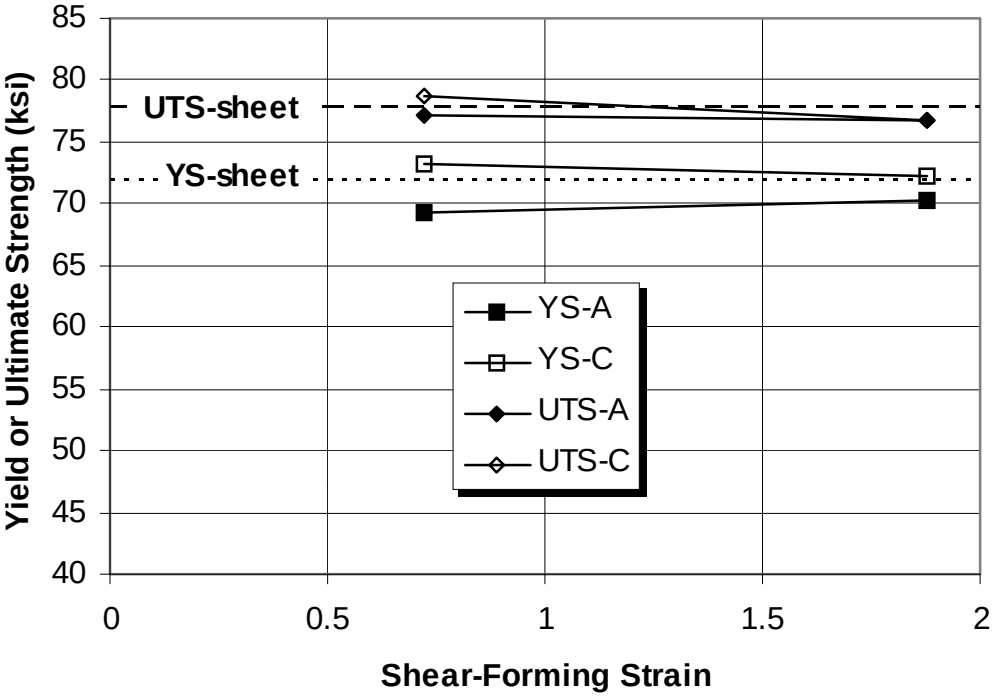

b) Reprocessed

Figure 20. Effect of shear-forming strain on yield strength (YS) and ultimate tensile strength (UTS) for C415-T8 shear formed cylinders in both the axial (A) and circumferential (C) orientations, compared with 0.090" C415-T8 sheet [23].

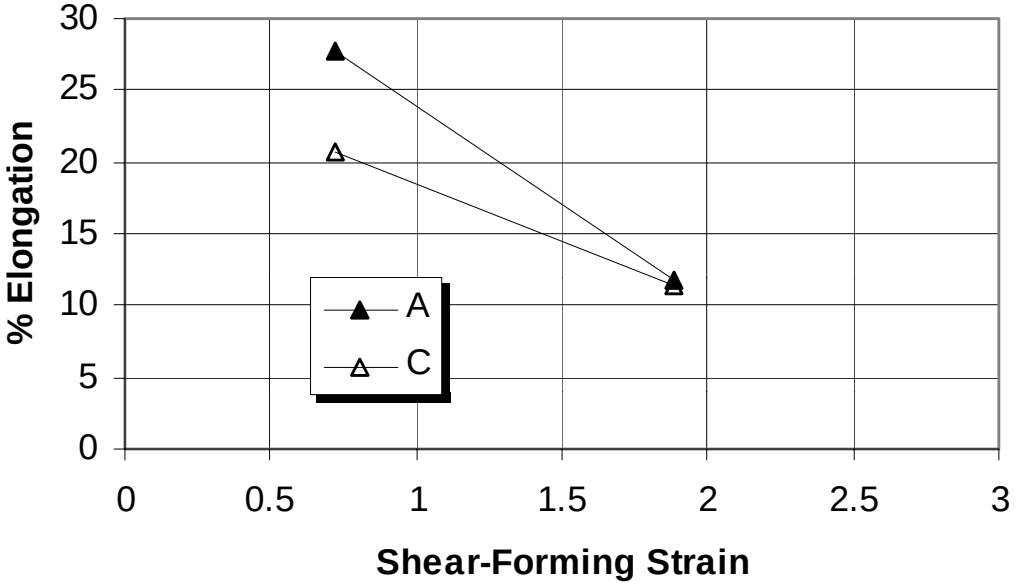

a) Direct-aged

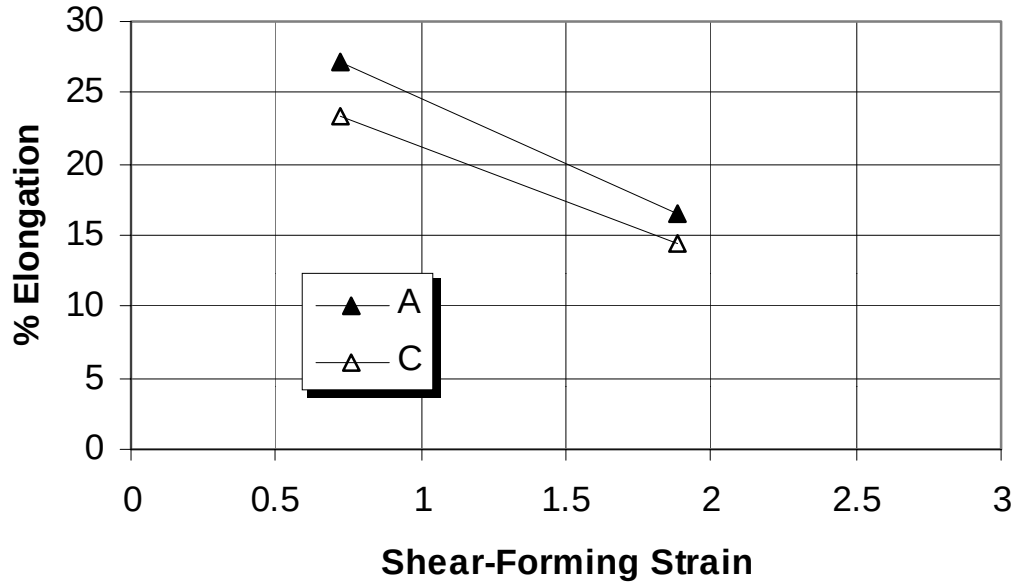

b) Reprocessed

Figure 21. Effect of shear-forming strain on ductility for C415-T8 shear formed cylinders in both the axial (A) and circumferential (C) orientations. The elongation was determined using fiducial marks.

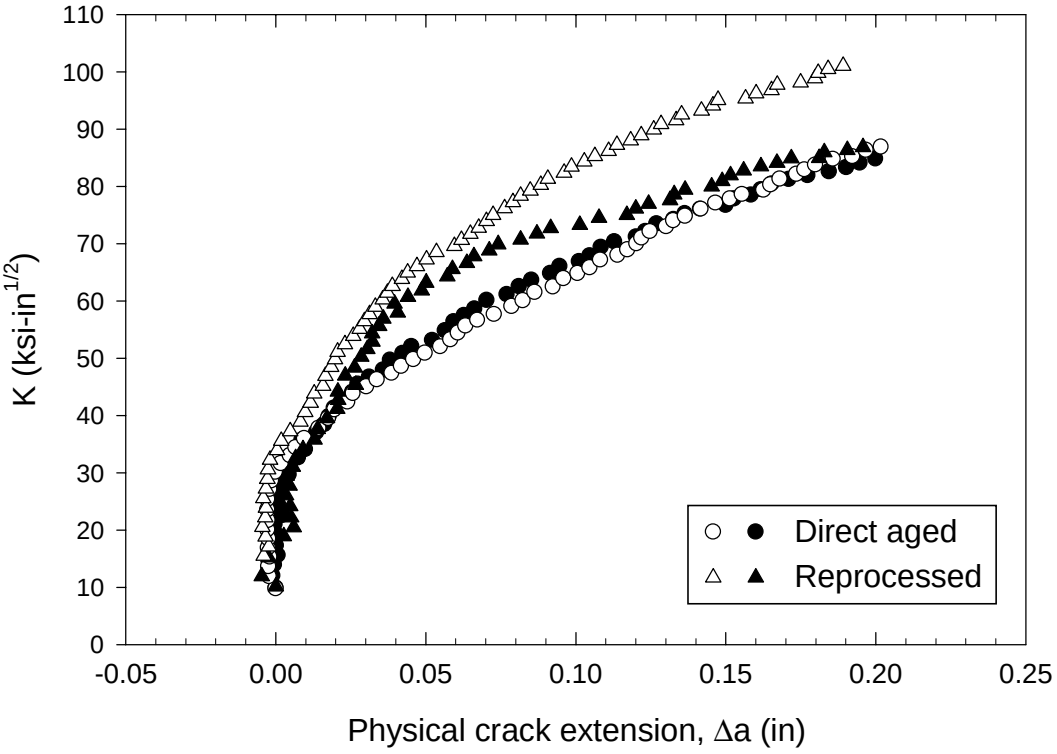

Figure 22. Crack growth curves for C415-T8 cylinder 1 for both the direct-aged and reprocessed conditions in the A-C orientation.

REPORT DOCUMENTATION PAGE

Form Approved
OMB No. 0704-0188

1. AGENCY USE ONLY *(Leave blank)*	2. REPORT DATE	3. REPORT TYPE AND DATES COVERED
	October 2000	Technical Memorandum

4. TITLE AND SUBTITLE
Microstructural and Mechanical Property Characterization of Shear Formed Aerospace Aluminum Alloys

5. FUNDING NUMBERS
522-63-41-02

6. AUTHOR(S)
Lillianne P. Troeger, Marcia S. Domack, and John A. Wagner

7. PERFORMING ORGANIZATION NAME(S) AND ADDRESS(ES)
NASA Langley Research Center
Hampton, VA 23681-2199

8. PERFORMING ORGANIZATION REPORT NUMBER
L-17952

9. SPONSORING/MONITORING AGENCY NAME(S) AND ADDRESS(ES)
National Aeronautics and Space Administration
Washington, DC 20546-0001

10. SPONSORING/MONITORING AGENCY REPORT NUMBER
NASA/TM-2000-210540

11. SUPPLEMENTARY NOTES
Troeger: NRC-Resident Research Associate, Langley Research Center, Hampton, VA
Domack and Wagner: Langley Research Center, Hampton, VA

12a. DISTRIBUTION/AVAILABILITY STATEMENT
Unclassified-Unlimited
Subject Category 26 Distribution: Standard
Availability: NASA CASI (301) 621-0390

12b. DISTRIBUTION CODE

13. ABSTRACT *(Maximum 200 words)*

Advanced manufacturing processes such as near-net-shape forming can reduce production costs and increase the reliability of launch vehicle and airframe structural components through the reduction of material scrap and part count and the minimization of joints. The current research is an investigation of the processing-microstructure-property relationships for shear formed cylinders of the Al-Cu-Li-Mg-Ag alloy 2195 for space applications and the Al-Cu-Mg-Ag alloy C415 for airframe applications. Cylinders which had undergone various amounts of shear-forming strain were studied to correlate the grain structure, texture, and mechanical properties developed during and after shear forming.

14. SUBJECT TERMS
Al-Cu-Li-Mg-Ag alloy; 2195, Al-Cu-Mg-Ag alloy; C415; mechanical properties; near-net-shape manufacturing; shear forming; microstructure; texture

15. NUMBER OF PAGES
45

16. PRICE CODE
A03

17. SECURITY CLASSIFICATION OF REPORT	18. SECURITY CLASSIFICATION OF THIS PAGE	19. SECURITY CLASSIFICATION OF ABSTRACT	20. LIMITATION OF ABSTRACT
Unclassified	Unclassified	Unclassified	UL